SPINAL MUSCULAR ATROPHY

Impaired prenatal motor axon development necessitates early therapeutic intervention in severe SMA

Lingling Kong[1], David O. Valdivia[1], Christian M. Simon[2]*, Cera W. Hassinan[1], Nicolas Delestrée[2], Daniel M. Ramos[1], Jae Hong Park[1], Celeste M. Pilato[1], Xixi Xu[1], Melissa Crowder[1], Chloe C. Grzyb[1], Zachary A. King[1], Marco Petrillo[3], Kathryn J. Swoboda[4], Crystal Davis[5], Cathleen M. Lutz[5], Alexander H. Stephan[6], Xin Zhao[7], Marla Weetall[7], Nikolai A. Naryshkin[7], Thomas O. Crawford[1,8], George Z. Mentis[2,9], Charlotte J. Sumner[1,10†]

Gene replacement and pre-mRNA splicing modifier therapies represent breakthrough gene targeting treatments for the neuromuscular disease spinal muscular atrophy (SMA), but mechanisms underlying variable efficacy of treatment are incompletely understood. Our examination of severe infantile onset human SMA tissues obtained at expedited autopsy revealed persistence of developmentally immature motor neuron axons, many of which are actively degenerating. We identified similar features in a mouse model of severe SMA, in which impaired radial growth and Schwann cell ensheathment of motor axons began during embryogenesis and resulted in reduced acquisition of myelinated axons that impeded motor axon function neonatally. Axons that failed to ensheath degenerated rapidly postnatally, specifically releasing neurofilament light chain protein into the blood. Genetic restoration of survival motor neuron protein (SMN) expression in mouse motor neurons, but not in Schwann cells or muscle, improved SMA motor axon development and maintenance. Treatment with small-molecule *SMN2* splice modifiers beginning immediately after birth in mice increased radial growth of the already myelinated axons, but in utero treatment was required to restore axonal growth and associated maturation, prevent subsequent neonatal axon degeneration, and enhance motor axon function. Together, these data reveal a cellular basis for the fulminant neonatal worsening of patients with infantile onset SMA and identify a temporal window for more effective treatment. These findings suggest that minimizing treatment delay is critical to achieve optimal therapeutic efficacy.

INTRODUCTION

New treatments for the neuromuscular disease spinal muscular atrophy (SMA) represent a forefront of emerging gene-targeting approaches potentially applicable to many neurogenetic disorders. Such treatments address the root cause of disease and thus hold the promise of marked efficacy, but early, nonreversible events in the pathogenic cascade may limit clinical benefit. Identifying the optimal timing of therapy and the basis for temporal constraints is key to therapeutic optimization.

SMA has historically been the most common inherited cause of infant and childhood mortality worldwide. It is caused by recessive mutations of the ubiquitously expressed survival motor neuron 1 (*SMN1*) gene with retention of its paralog, *SMN2*, in variable copy number (*1*). A translationally synonymous C>T substitution in exon 7 of *SMN2* results in alternative splicing (*2*, *3*), with most mature *SMN2* transcripts lacking exon 7 and encoding a truncated, unstable SMNΔ7 protein. Patients with the most frequent and severe infantile onset form of SMA, labeled "Type 1," generally carry two copies of *SMN2* and experience profound axial, limb, and bulbar muscle weakness within weeks or months of birth (*4*, *5*). Patients with milder forms of SMA, labeled Types 2 and 3, often have three or four copies of *SMN2* (*6*).

Rapid advances in the development of gene targeting therapeutics have led to three new SMA therapies that induce SMN expression, each with a distinct mechanism of action, pharmacokinetics, and bio-distribution. The *SMN2* pre-mRNA splice-switching antisense oligonucleotide (ASO) nusinersen (Spinraza) was approved for patients of all ages in 2016 (*7*, *8*). Adeno-associated virus 9–mediated delivery of an *SMN* cDNA onasemnogene abeparvovec (Zolgensma) was approved by the Food and Drug Administration in 2019 for patients with SMA aged less than 2 years (*9*). Risdiplam (Evrydsi), an orally administered, central nervous system–bioavailable splice-switching small molecule (*10*), was approved in 2020. These therapies show notable efficacy in some patients, but clinical response is variable, ranging from normalization of early motor milestone achievement to little or no detectable improvement in motor function (*11*). Earlier age of treatment initiation is a critical factor: Infants treated with nusinersen pre-symptomatically before 6 weeks of life (*12*) respond much better than infants treated post-symptomatically starting between 1 and 7 months (*7*).

G. Werdnig in 1891 first identified a spinal cause for the muscle atrophy of SMA, and coined the name "spinale Muskelatrophie,"

[1]Department of Neurology, Johns Hopkins University School of Medicine, Baltimore, MD 21205, USA. [2]Center for Motor Neuron Biology and Disease, Department of Pathology and Cell Biology, Columbia University, New York, NY 10032, USA. [3]Biogen, Cambridge, MA 02142, USA. [4]Center for Genomic Medicine, Department of Neurology, Massachusetts General Hospital, Harvard Medical School, Boston, MA 02114, USA. [5]Genetic Resource Science, The Jackson Laboratory, Bar Harbor, ME 04609, USA. [6]F. Hoffmann–La Roche Ltd., pRED, Pharma & Early Development, Roche Innovation Center Basel, Basel CH-4070, Switzerland. [7]PTC Therapeutics, 100 Corporate Court, South Plainfield, NJ 07080, USA. [8]Department of Pediatrics, Johns Hopkins University School of Medicine, Baltimore, MD 21205, USA. [9]Department of Neurology, Columbia University, New York, NY 10032, USA. [10]Department of Neuroscience, Johns Hopkins University School of Medicine, Baltimore, MD 21205, USA.
*Present address: Carl-Ludwig-Institute for Physiology, Leipzig University 04103, Germany.
†Corresponding author. Email: csumner1@jhmi.edu

with his description of markedly diminished size of SMA ventral roots (VRs) in patient autopsy tissue (*13*). Over a century later, the cellular mechanisms underlying this pathology and the relative contributions of impaired development and/or degeneration remain poorly defined. Motor axons must be of large radial caliber and surrounded by compact myelin to rapidly conduct action potentials. Developmental acquisition of these axons involves a multistep morphogenetic process of radial growth and sorting by Schwann cells [fig. S1 and (*14*, *15*)]. Initially, only a few Schwann cells surround bundles of small, directly abutting axons. Individual axon radial growth leads to their ensheathment by processes of Schwann cell cytoplasm. Further radial expansion coinciding with Schwann cell proliferation leads to a 1:1 segregation between axons and Schwann cells and continued growth beyond 1 to 2 μm results in formation and proportional thickening of the compact myelin sheath. Unmyelinated autonomic or sensory axons remain small and ensheathed in polyaxonal Remak bundles.

In this study, we characterized this complex morphogenetic cascade in tissues from both patients with SMA and a mouse model of severe SMA. Our studies identify a marked delay of SMA motor axon radial growth and sorting, failed ensheathment of many axons, and subsequent degeneration after birth of those axons that lag the most in this developmental sequence. These findings provide a cellular basis for the limited temporal window of highly efficacious SMN induction therapy and argue for steps to minimize neonatal treatment delays.

RESULTS

Impaired development and degeneration of human SMA motor neuron axons

To understand early pathological events in patients with SMA, we performed dissections of spinal cord, VRs, dorsal roots (DRs), peripheral nerve, and muscle during expedited autopsies of patients with severe SMA and age-matched controls (table S1). As expected, most myofibers in the clinically affected iliopsoas (Fig. 1, A and B, and fig. S2A) and intercostal (fig. S2, B to D) muscles were hypotrophic in SMA cases, whereas myofiber size was minimally changed in the clinically less affected diaphragm muscle (fig. S2, E to G). SMA VRs, which contain the large, myelinated motor axons, were grossly thin (fig. S3A), and VR cross-sectional area was reduced at the lumbar level (Fig. 1, C and D). About two- to threefold fewer myelinated axons were visualized by light microscopy in SMA thoracic, upper, and lower lumbar VRs (Fig. 1, E and F). Examination of the VRs of patients diagnosed with SMA Type 1, Type 2, and controls, stratified by age, suggested an increase in VR size and myelinated axon number in controls over the first months and years of life, but these parameters were diminished in all SMA cases (fig. S3, B to F). No differences were observed in sensory DRs or the clinically less affected phrenic nerve (fig. S3, H to M).

A reduction of large myelinated axon numbers in SMA VRs has been attributed to their degeneration (*16*), but an alternative possibility is that they are not developmentally acquired. Immunostaining for neuron-specific class III β-tubulin (Tuj1) in control VRs revealed that most Tuj1-immunoreactive punctae were encircled by myelin protein zero (MPZ), consistent with their identity as large myelinated axons (Fig. 1, G and H). In SMA VRs, some $Tuj1^+$ punctae were encircled by MPZ, but many lacked MPZ staining (Fig. 1, G and H). Most of the small punctae not encircled by MPZ stained robustly for growth-associated protein 43 (GAP43) (Fig. 1G and fig. S3N), known to be expressed by developing axons and nonmyelinating Schwann cells (*17*, *18*). In addition, more of these small axons not encircled by MPZ stained for neurofilament light chain (NF-L), which is expressed by axons early in development, but not phosphorylated neurofilament heavy chain (pNF-H) (Fig. 1, I and J), which is expressed later in development (*19*). The presence of numerous small axons in SMA VRs raises the possibility that many SMA motor axons fail to grow sufficiently to become myelinated by Schwann cells. Normal proportions of myelinated and unmyelinated axons were observed in SMA DRs and phrenic nerve (fig. S3, O to Q).

To characterize the progression of human VR axon developmental morphologic stages, we used transmission electron microscopy (EM) to image VRs and quantify the fraction of axons of different types. On the basis of their appearance and relationship to surrounding Schwann cells, axons were assigned to one of four groups (fig. S1). Unmyelinated axons directly abutting one another in polyaxonal pockets were categorized as "abutting," unmyelinated axons surrounded by Schwann cell cytoplasm within a polyaxonal pocket were categorized as "ensheathed," unmyelinated axons that had established a 1:1 relationship with a Schwann cell were categorized as "segregated," and segregated axons surrounded by any identifiable compact myelin were categorized as "myelinated." In control upper and lower lumbar VRs, most axons were large and myelinated, fitting the profile characteristic of alpha motor neuron (MN) axons (Fig. 2, A and B). A proportion of axons were unmyelinated in control upper lumbar VRs, but they were ensheathed within Remak bundles, consistent with the mature autonomic axons known to make up about 20% of VR axons at this spinal segment (*20*). In SMA upper and lower lumbar VRs, the proportion of myelinated axons was reduced (Fig. 2, A and B), and the diameter of these myelinated axons was diminished (upper lumbar mean: control = 5.37 ± 1.50 versus SMA = 2.87 ± 0.75, $P < 0.0001$; lower lumbar mean: control = 5.96 ± 1.32, SMA = 4.06 ± 0.82, $P < 0.0001$, unpaired *t* tests) (Fig. 2, C and D). Examination of individual control cases stratified by increasing age demonstrated an increase of VR myelinated axon diameter during normal development, but in SMA cases, myelinated axon caliber was reduced, with few SMA axons reaching a diameter greater than 5 μm (Fig. 2, C and D, and fig. S3, D and G). G ratios (ratio of the inner to outer diameter of the myelin sheath) of control and SMA myelinated VR axons were equivalent, indicating an appropriate myelin thickness for axon size [upper lumbar: control = 0.75 ± 0.04 ($n = 3$); SMA = 0.74 ± 0.04 ($n = 4$); $P = 0.80$ and lower lumbar: control = 0.75 ± 0.05 ($n = 6$); SMA = 0.76 ± 0.03, ($n = 6$); $P = 0.49$, unpaired *t* tests] (Fig. 2, C and D). As G ratio would be expected to decrease in the setting of axon atrophy, the absence of change argues in favor of a developmental impairment of radial axon growth.

A high percentage of axons present in SMA VRs were unmyelinated, small, and abutting (Fig. 2, A and B, and fig. S3, R to U). Axons of this morphology were very rarely seen in control VRs, even as early as 1 day of life (fig. S3, R and T), but are well documented in human fetal nerve (*21*, *22*). This preponderance of directly abutting axons was also found in SMA intercostal nerves (fig. S4A), where demonstrably increased staining for GAP43 (fig. S4B) indicated that immature axons may be present in both proximal and distal segments. Intramuscular nerve with fetal morphology has also been described previously in two patients with severe infantile SMA (*23*). Although the absolute number of myelinated axons was similarly

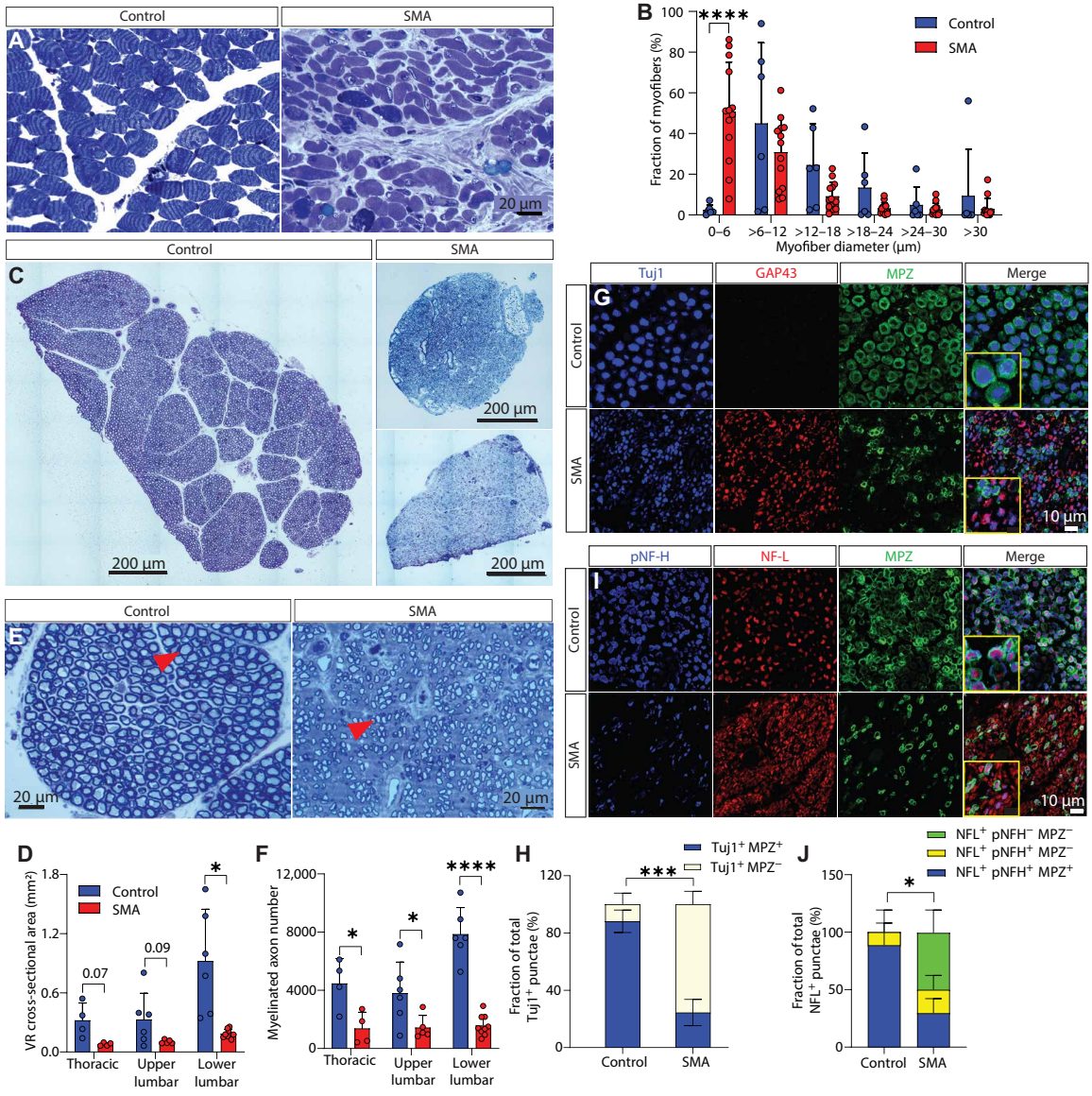

Fig. 1. Myofiber and VR hypotrophy in patients with SMA. (**A**) Toluidine blue–stained cross sections of iliopsoas muscles from CNTL 12-05 (19 months, left) and SMA 10-01 (15 months, right). (**B**) Histogram of iliopsoas myofiber diameter: controls (ages: 0.03 to 168 months, $n = 6$) and SMA Type 1 (ages: 1.75 to 36 months, $n = 13$). (**C**) Toluidine blue–stained cross sections of L5 VRs from CNTL 17-01 (9 months, left), SMA 98-16 (9 months, upper right), and SMA 17-03 (0.5 months, lower right). (**D**) Average VR cross-sectional area: controls (ages: 0.03 to 168 months, $n = 4$ to 6) and SMA Type 1 cases (ages: 0.5 to 72 months, $n = 4$ to 8). (**E**) High-magnification images of VRs from CNTL 17-01 (9 months, left) and SMA 98-16 (9 months, right). Arrowheads indicate examples of myelinated axons. (**F**) Average total VR myelinated axon number. (**G**) Confocal images of lower lumbar VRs stained with Tuj1 (blue), GAP43 (red), and MPZ (green) from CNTL12-05 (19 months) and SMA11-01 (1.8 months). (**H**) Percentage of Tuj1$^+$ punctae with or without encircling MPZ staining in controls (ages: 0.03 to 19 months, $n = 3$) and SMA Type 1 cases (ages: 1.75 to 16 months, $n = 5$). (**I**) Confocal images of lower lumbar VRs stained with pNF-H (blue), NF-L (red), and MPZ (green) from CNTL08-01 (4 months) and SMA17-03 (0.5 months). (**J**) Percentage of pNF-H$^+$/NF-L$^+$ or pNF-H$^-$/NF-L$^+$ punctae with or without encircling MPZ staining in VRs of control (ages: 0.03 to 9 months, $n = 3$) and SMA Type 1 cases (ages: 0.5 to 7 months) (* represents the difference between control and SMA in the pNF-H$^-$/NF-L$^+$/MPZ$^-$ and pNF-H$^+$/NF-L$^+$/MPZ$^+$ groups). Data represent means and SD. Statistical analysis was performed using Mann-Whitney test for (B) and unpaired *t* test for (D), (F), (H), and (J). Significance: $^*P \leq 0.05$, $^{***}P < 0.001$, $^{****}P < 0.0001$.

reduced in all SMA cases (fig. S3, C and F), their proportion relative to unmyelinated axon types appeared to be increased in those cases with increased age and disease duration (fig. S3, R and T). This could indicate preferential loss of immature axons over time. Only small percentages of myelinated axons were actively degenerating [defined by the presence of a myelin ovoid (Fig. 2A, red arrow)] in both control (CNTL) and SMA cases (Fig. 2, E and F), but between ~15 and 40%, of small, unmyelinated axons were degenerating [as defined by loss of axonal cytoskeletal integrity (Fig. 2A, blue arrow)] in SMA cases (Fig. 2, E and F). Depletion of MN soma numbers was also seen in upper and lower lumbar SMA spinal cords (Fig. 2, G and H, and fig. S4, C to E), indicating that proximal axonal loss was associated with commensurate cell body loss. Median MN somal size, like axonal caliber, was significantly reduced in the lower

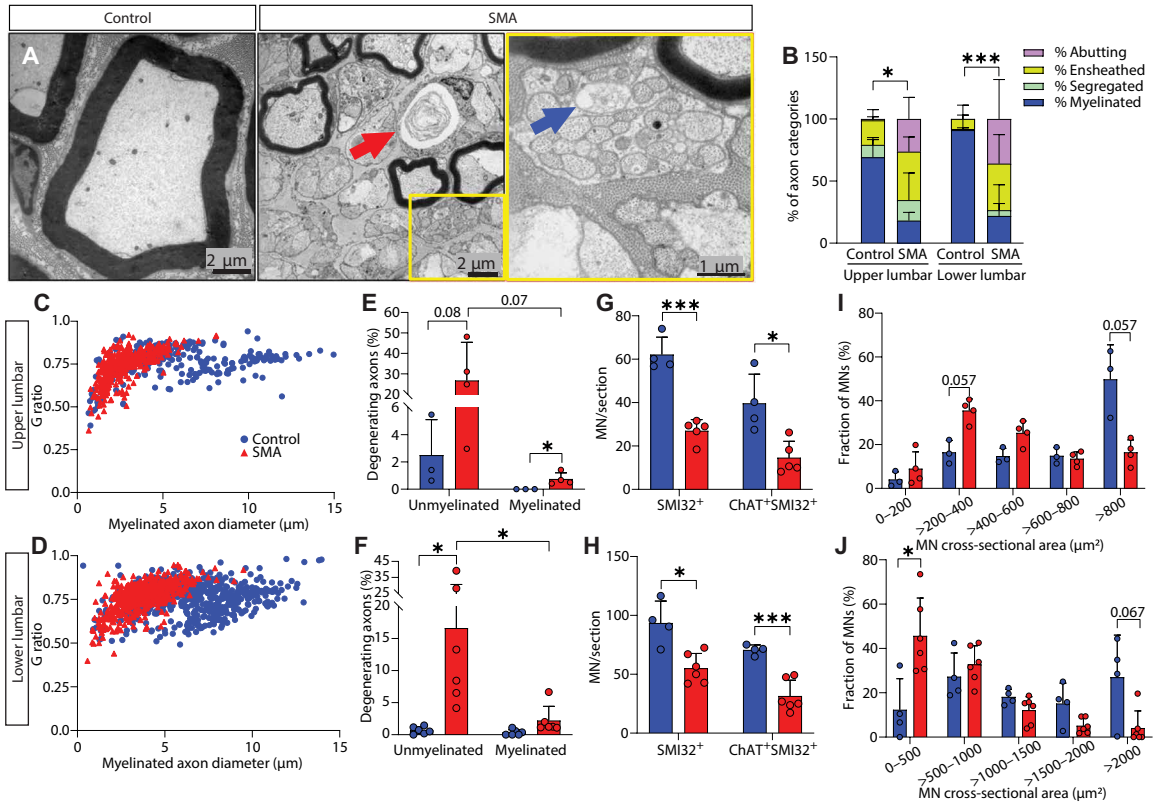

Fig. 2. Immature morphologies of SMA VR axons. (**A**) EM images of axons in VRs from CNTL12-05 (19 months, left) and SMA11-01 (1.8 months, middle and right). The right panel is a higher-magnification view of the yellow square in the middle panel. The red arrow indicates a degenerating myelinated axon; the blue arrow indicates a degenerating, abutting axon. (**B**) Average percentage of axons of different categories in upper lumbar VRs: controls (ages: 0.03 to 36 months, $n = 3$) and SMA Type 1 (ages: 1.75 to 72 months, $n = 5$) and lower lumbar VRs: controls (ages: 0.03 to 168 months, $n = 6$) and SMA Type 1 (ages: 0.5 to 72 months, $n = 6$) (* indicates significance for the myelinated axon group). (**C** and **D**) Axon diameters and G ratios of VR motor axons in upper lumbar (CNTL: $n = 3$, SMA: $n = 4$) (C) and lower lumbar (CNTL: $n = 6$, SMA: $n = 6$) (D) VRs. (**E** and **F**) Average percentage of degenerating unmyelinated and myelinated axons in control and SMA Type 1 upper lumbar (CNTL, ages: 0.03 to 36 months, $n = 3$; SMA, ages: 1.75 to 72 months, $n = 4$) (E) and lower lumbar (CNTL: ages: 0.03 to 168 months, $n = 6$; SMA, ages: 0.5 to 72 months, $n = 6$) (F) VRs. (**G** and **H**) Number of MNs per section determined by NF-H (SMI32) and ChAT staining in upper lumbar spinal cord [control (ages: 0.03 to 168 months, $n = 4$) and SMA Type 1 (ages: 1.75 to 72 months, $n = 5$)] (G) and lower lumbar spinal cord [control (ages: 0.03 to 168 months, $n = 4$) and SMA (ages: 0.5 to 72 months, $n = 6$)] (H). (**I** and **J**) MN size distribution in the upper lumbar spinal cord [control (ages: 0.03 to 9 months, $n = 3$) and SMA Type 1 (ages: 1.75 to 4 months, $n = 4$)] (I) and lower lumbar spinal cord [control (ages: 0.03 to 19 months, $n = 4$) and SMA (ages: 0.5 to 16 months, $n = 6$)] (J). Data represent means and SD. Statistical analysis was performed using unpaired *t* test for (B) to (H) and Mann-Whitney test for (I) and (J). Significance: $^*P \leq 0.05$; $^{***}P < 0.001$.

lumbar spinal cord compared to age-matched controls (upper lumbar: control = 901.21 ± 229.08 μm^2; SMA = 531.91 ± 81.69 μm^2, $P = 0.10$; lower lumbar: control = 1484.16 ± 513.24 μm^2; SMA = 633.38 ± 149.01 μm^2, $P = 0.009$, unpaired *t* tests) (Fig. 2, I and J, and fig. S4F).

Precipitous neonatal degeneration follows delays of axon development in SMA mice

To characterize SMA motor axons over the course of development, we examined VRs from severe SMA mice (SMAΔ7) at fetal and postnatal time points. We have previously demonstrated that lumbar 1 (L1) alpha MN loss occurs postnatally and is more severe than L5 MN loss in this model (*24*). We thus compared proximal L1 and L5 VRs by light microscopy. Whereas L1 VR size increased over developmental time in wild-type (WT) mice, it was reduced in SMA mice starting at embryonic day (E) 17.5 and showed little growth through postnatal day (P) 14 (slopes μm^2/day: WT = 353.3 versus SMA = 79.28, $P < 0.0001$, linear regression analysis) (Fig. 3A). The acquisition of myelinated axons was also reduced in SMA L1 VRs (slopes axon number/day: WT = 20.32 versus SMA = 13.06, $P = 0.01$, linear regression analysis) (Fig. 3B). Similar patterns were observed in thoracic (T) 10 VRs (fig. S5, A to C). In contrast, differences in L5 VRs occurred only at disease end stage (P14) (Fig. 3, C and D). No differences were observed in L1 DRs at P14 (fig. S5, D to F).

Reconstruction of whole VRs using a montage of overlapping EM images enabled assessment of the absolute number of axons of all types (*25*) and their developmental morphologies (Fig. 3, E to Q). At E13.5, the total number of axons (Fig. 3G) and their size (Fig. 3L) were equivalent in WT and SMA L1 VRs, and more than 90% of axons were abutting, consistent with this early developmental stage. By E17.5, WT VRs contained an increased number of ensheathed and segregated axons (Fig. 3M), but SMA L1 VRs retained an increased number of very small, abutting axons (axon number: WT = 287 ± 223; SMA = 541 ± 140, $P = 0.04$, unpaired *t* test) (Fig. 3G), a higher number of axons per bundle (Fig. 3H), and a reduced number of VR Schwann cell nuclei (Fig. 3I), together indicating slowed axon–Schwann cell sorting. Only a very small fraction of these abutting

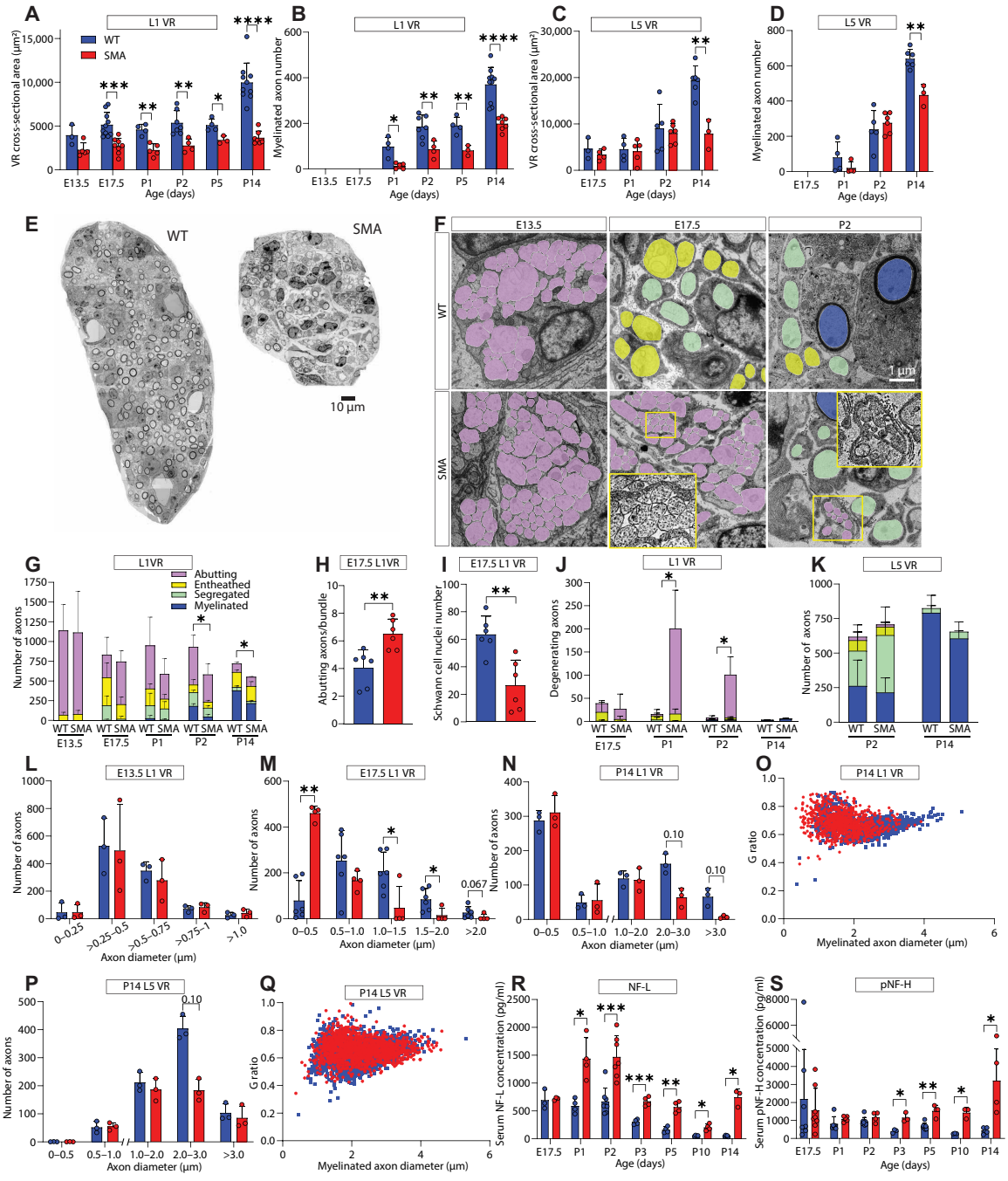

Fig. 3. Impaired motor axon radial growth and sorting begin prenatally and are associated with rapid neonatal degeneration in SMA mice. (**A** to **D**) VR cross-sectional area (A and C) and VR myelinated axon number in L1 (A and B) and L5 (C and D) VRs of SMAΔ7 mice (WT: $n = 3$ to 10; SMA: $n = 3$ to 8). (**E**) Representative reconstructed EM images of L1 VRs acquired at 8000× from WT and SMA mice at P2. (**F**) Representative EM images of L1 VR axons from E13.5 to P2. Pseudocoloring: pink = abutting axons; yellow = ensheathed, unmyelinated axon; green = segregated, unmyelinated axons; blue = myelinated axons. (**G**) Total number of axons of different morphological types in L1 VRs from E13.5 to P14 (WT: $n = 3$ to 6; SMA: $n = 3$ to 6) (* indicates significance for the total number of axons). (**H** and **I**) The average number of abutting axons per bundle (H) and number of Schwann cell nuclei per L1 VR (I) at E17.5 ($n = 6$ each). (**J**) Total number of degenerating axons from each axon category in L1 VRs from E17.5 to P14 ($n = 3$ to 4 in each group) (* indicates significance for the degenerating, abutting axon group). (**K**) Total number of axons of different morphological types in L5 VRs at P2 and P14 ($n = 3$ each). (**L** to **N**) Histogram of axon diameter in L1 VRs at E13.5 ($n = 3$ each) (L), E17.5 (WT: $n = 6$, SMA: $n = 4$) (M), and P14 ($n = 3$ each) (N). (**O**) Axon diameter–G ratio histogram of myelinated axons in L1 VRs at P14 ($n = 3$ each). (**P**) Histogram of diameter of all axons in L5 VRs at P14 ($n = 3$ each). (**Q**) Axon diameter–G ratio histogram of myelinated axons in L5 VRs at P14 ($n = 3$ each). (**R** and **S**) Serum NF-L (WT: $n = 3$ to 8; SMA: $n = 3$ to 7) (R) and pNF-H ($n = 3$ to 8 each) (S) concentrations in SMAΔ7 mice from E17.5 to P14. Data represent means and SD. Statistical analysis was performed using unpaired t test in (A) to (D), (G) to (K), (R), and (S) and Mann-Whitney test in (L) to (N) and (P). Significance: $^*P \leq 0.05$; $^{**}P < 0.01$; $^{***}P < 0.001$, $^{****}P < 0.0001$.

axons were larger than 1 μm in diameter in both WT and SMA mice (WT = 0.84 ± 0.37%, SMA = 1.70 ± 2.30%, $P = 0.40$, unpaired t test). At E17.5, there were no signs of axonal degeneration, but at P1 and P2, multiple, abutting L1 VR axons showed degenerative morphologies (Fig. 3J), and by P2, there was a 37.5% decrease in the total number of L1 VR axons in SMA compared to WT (Fig. 3G). No differences in the distribution of axon types were observed in L5 VRs at P2 or P14 (Fig. 3K).

The observed loss of L1 VR axons at P1 and P2 was followed by MN somal loss in the ventral horn of the L1 spinal segment (fig. S6, A to C) and was concurrent with distal axon terminal loss at the neuromuscular junction (NMJ) (defined as <25% synaptophysin coverage of the NMJ endplate) in the L1 paraspinal muscles [PS, specifically the multifidus, longissimus, and iliocostalis muscles, known to be innervated by dorsally projecting alpha motor axons of the same spinal segment (*26*)] (fig. S6, D to H). Loss of NMJ innervation implies that proximal L1VR axon loss specifically involves motor axons, but because L1 VRs contain both somatic MN axons and preganglionic autonomic axons (*27*), we cannot exclude some concomitant degeneration of autonomic axons. The loss of L1 PS NMJ innervation was followed by impaired growth of L1 PS myofibers at P5 and P10 (fig. S6, N and O). Variable NMJ denervation was observed in L5 PS at P14 only (fig. S6, I to M), and no impairment of L5 PS myofiber growth was observed (fig. S6P).

In contrast to earlier time points, between P2 and P14, there was only moderate additional loss of proximal L1 VR axons (Fig. 3, G and J) in SMA mice, and the remaining axons acquired more mature morphologies as well as increased diameter (Fig. 3, N and O). Despite this, median diameter of myelinated axons in the SMA L1 VR was smaller at P14 (WT = 2.45 ± 0.11 μm, $n = 3$; SMA = 1.65 ± 0.34 μm, $n = 4$, $p = 0.01$, unpaired t test) (Fig. 3, L to O) with a particular paucity of myelinated axons greater than 3 μm. Median G ratios were equivalent (WT = 0.67 ± 0.02, $n = 3$; SMA = 0.68 ± 0.02, $n = 4$, $P = 0.28$, unpaired t test), indicating an appropriate myelin thickness for axon size (Fig. 3O). The less affected L5 VR myelinated axons showed no alteration of diameter or G ratios at P14 (Fig. 3, P and Q).

Serum biomarkers of axonal degeneration

As NFs have been proposed as biomarkers of degeneration in SMA and other neurodegenerative diseases (*28*), we examined NF-L and pNF-H concentrations in the serum of SMA and WT littermate mice of different ages. Serum NF-L concentrations were maximally increased in SMA mice compared to WT mice at P1 and P2 (Fig. 3R), temporally paralleling the neonatal L1 VR axon loss detected histologically. pNF-H concentrations were not elevated at these time points (Fig. 3S) consistent with the immaturity of the axons that degenerate during this neonatal interval. After P2, NF-L concentrations steadily declined until P10 but remained higher than controls. pNF-H was increased in SMA mice compared to controls starting at P3. Concurrent increases of NF-L and pNF-H suggest degeneration of more mature motor axons at later time points.

Delayed SMA axon development impairs motor axon function

To evaluate whether the identified abnormalities of SMA motor axons are associated with alterations of function, we evaluated NMJ structure histologically followed by electrophysiological characterization of ex vivo spinal cord/muscle preparations (*29*). The percentage of innervated NMJs was determined in the quadratus lumborum (QL) muscle, which is innervated by L1 to L3 MNs (*29*), and the tibialis anterior (TA) muscle, which is innervated by L4 and L5 MNs (Fig. 4, A to C). In the QL muscle, there was a modest 8.6% reduction of innervated NMJs in SMA compared to WT mice at birth and subsequent losses to 25% at P3, followed thereafter by a slower rate of decline of innervation percentage (Fig. 4B). In contrast, the TA muscle remained innervated at all time points (Fig. 4C).

Stimulation of L1 VR motor axons with electromyographic recording at the QL muscle was compared to L4 VR stimulations recording at the TA muscle. At P1, L4 SMA and WT motor axons showed equivalent compound muscle action potential (CMAP) amplitudes, which represent the summated voltage responses from the individual muscle fiber action potentials generated by the most rapidly conducting axons (Fig. 4, D and E). The latency to initiation of the CMAP response was also equivalent in WT and SMA L4 VR axons at this time point. This latency is largely a function of the axonal conduction velocity (CV), which can be approximated from the latency and the measured distance between stimulating and recording electrodes (Fig. 4, D to F). Despite only a modest loss of innervated NMJs in the QL muscle at P1, the amplitude of the CMAP was already reduced by about 2.5-fold in SMA mice compared to WT littermates (Fig. 4, D and E). This may reflect the reduced acquisition of myelinated axons already evident at this time point (Fig. 3B) and suggests that many muscle fibers are innervated by small axons that do not contribute to the CMAP. We also observed that the CV of SMA L1 axons was reduced (Fig. 4, D and F). This reduction was not due to slow NMJ transmission, as similar slowing was seen with retrograde stimulation of the intramuscular nerve with recording of nerve action potential at the VR (fig. S7, A to I). Instead, the reduced CV likely reflects the reduced diameter of myelinated axons at this spinal level. Of note, during 25% of L1 VR stimulations performed at P5, and 100% of stimulations performed at P11, we observed a variable number of small-amplitude responses at prolonged latencies well after the initial peak (fig. S7J), which increased the duration of the CMAP in SMA mice at P11 (fig. S7K).

Between P1 and P11, the CMAP amplitude of WT L1 motor axons increased by 276% and their CV increased by 337% (Fig. 4, D to F), consistent with the rapid acquisition of newly myelinated axons and radial growth of existing myelinated axons during this interval. In contrast, the CMAP amplitude of SMA L1 VR declined by 36% between P1 and P5, and between P5 and P11, it declined an additional 15% (slopes mV/day: WT = 0.19 versus SMA = −0.01, $P < 0.0001$, linear regression analyses) (Fig. 4, D and E). SMA motor axon CVs increased between P1 and P11 in L1 (Fig. 4, D and F), consistent with the increased radial growth of the few acquired myelinated axons (Fig. 3, N and O), but CV remained twofold lower than WT motor axons at P11 (slopes mm/ms/day: WT = 0.10 versus SMA = 0.03, $P < 0.0001$, linear regression analyses). Together, these data indicate that L1 motor axons exhibit functional deficits in action potential conduction consistent with their morphological developmental impairments.

Loss of SMN in MNs impairs motor axon development

The process of axon radial sorting, growth, and myelination requires complex molecular interactions between axons and Schwann cells and can be disrupted by alterations of proteins expressed by each cell type (*14*, *15*). To characterize the contribution of different cell types to the motor axon developmental pathology of SMA, we examined SMA mice expressing the well-validated Cre recombinase–inducible *Smn* hybrid allele (Smn^{Res}) (*30*) together with Cre recombinase

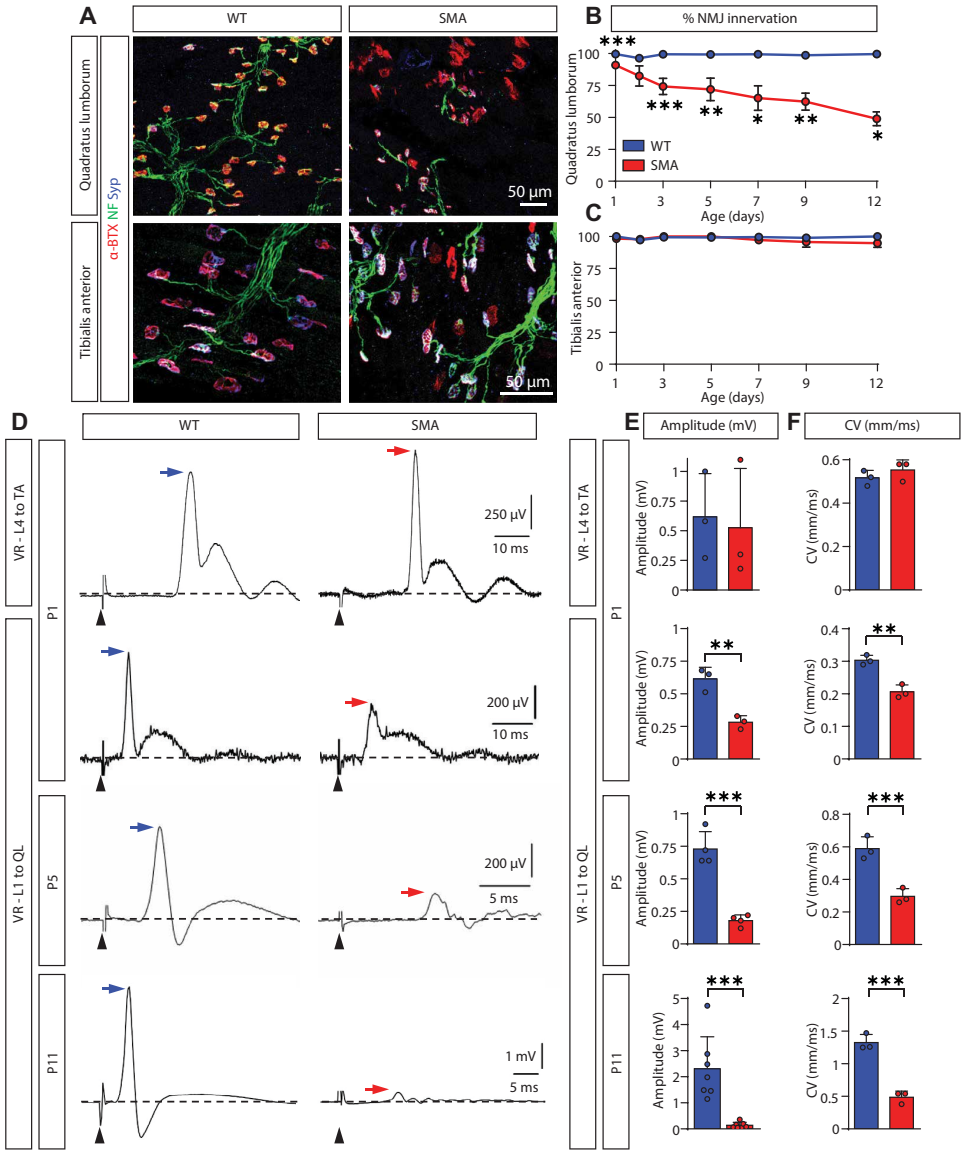

Fig. 4. Time course of NMJ denervation and electrophysiological abnormalities of vulnerable SMA motor neuron axons. (**A**) NMJ staining with α-bungarotoxin (α-BTX, red), synaptophysin (Syp, blue), and neurofilament (NF, green) in QL and TA muscles in P11 WT and SMA mice. (**B** and **C**) Quantification of NMJ innervation in QL (B) and TA (C) muscles in WT ($n = 3$) and SMA ($n = 3$ to 5) mice from P1 to P12. (**D**) CMAP recordings from the TA muscle after L4 VR stimulation at P1 and CMAP recordings from the QL muscle after L1 VR stimulation in WT and SMA mice at P1, P5, and P11 and in WT and SMA mice. Arrows indicate maximum CMAP amplitude. Black arrowheads indicate the stimulus artifact. Scale bars shown in SMA also apply for the corresponding WT. (**E** and **F**) Quantification of CMAP amplitude (E) and nerve CV (F) for QL and TA muscle recordings shown in (D) ($n = 3$ to 7 each). Data represent means and SD. Statistical analysis in (B), (C), (E), and (F) was performed using unpaired *t* test. Significance: $^{*}P \leq 0.05$; $^{**}P < 0.01$; $^{***}P < 0.001$.

under control of (i) the choline acetyltransferase (ChAT) promoter [expressed in MNs beginning at E12.5 (*31*)], (ii) the desert hedgehog (Dhh) promoter [expressed in Schwann cell progenitor cells beginning at E12 (*32*)], or (iii) the MyoD promoter [expressed in myofibers beginning at E9.75 (*33*)]. We have previously described the generation and phenotype of the $ChAT^{Cre}$ and $MyoD^{iCre}$ mice (*34*), both of which show phenotypic improvements in motor behavior and survival. Only $ChAT^{Cre}$ mice show increased MN maintenance, however. To characterize Dhh^{Cre} mice, we confirmed that Dhh^{Cre} is expressed specifically in Schwann cells and Sertoli cells, as previously described, and not in MNs (fig. S8A). We also demonstrated that Dhh^{Cre} mice express increased amounts of full-length *SMN* mRNA in sciatic nerve by using reverse transcription–quantitative polymerase chain reaction (fig. S8, B and C). Behavioral characterization of the Dhh^{Cre} mice showed no improvement in survival or motor behavior (fig. S8, D and E).

We examined the impact of these cell type–specific increases of SMN expression upon L1 VR motor axon development and degeneration. Increased expression of SMN in MNs in $ChAT^{Cre}$ mice increased VR size and VR axon maturation (Fig. 5, A to H) and resulted in decreased NF-L concentrations in the serum (Fig. 5, I and J), suggesting prevention of early axonal degeneration. These histological improvements were associated with normalization of CMAP amplitudes and CVs at P11 (Fig. 5, K to M). This contrasts with the absence of improvement in motor axon development or survival in Dhh^{Cre} mice and only modest improvement in axon radial growth in $MyoD^{iCre}$ mice at P14 (fig. S9). Together, these data indicate that early impairments of motor axon radial growth and survival are principally determined by deficient SMN expression in MNs.

Fetal initiation of SMN induction therapeutics prevents early motor axon degeneration in severe SMA mice

To examine the necessary timing of changes in SMN expression on motor axon development and degeneration, we treated SMAΔ7 mice with the small-molecule splice modifier SMN-C3 (*35*) starting at selected prenatal and postnatal time points. SMN-C3 has wide tissue distribution and effectiveness in increasing full-length SMN expression in SMAΔ7 mice. We postulated that embryonic SMA mice could be treated by dosing pregnant dams by intraperitoneal injection. SMN-C3 concentrations in embryonic mouse brain and liver collected from normal littermate mice 1 and 6 hours after injection of vehicle or SMN-C3 (3 mg/kg) delivered to a pregnant dam at E13.5 (fig. S10, A and B) were similar to those previously observed in SMAΔ7 mice treated postnatally with a known efficacious dose of 1 mg/kg (*35*). Efficacious SMN-C3 drug concentrations were also observed in brain and spinal cord tissues from P10 SMA mice that were treated both prenatally and with daily intraperitoneal postnatal SMN-C3 starting at E13.5 (fig. S10, C and D). Similar

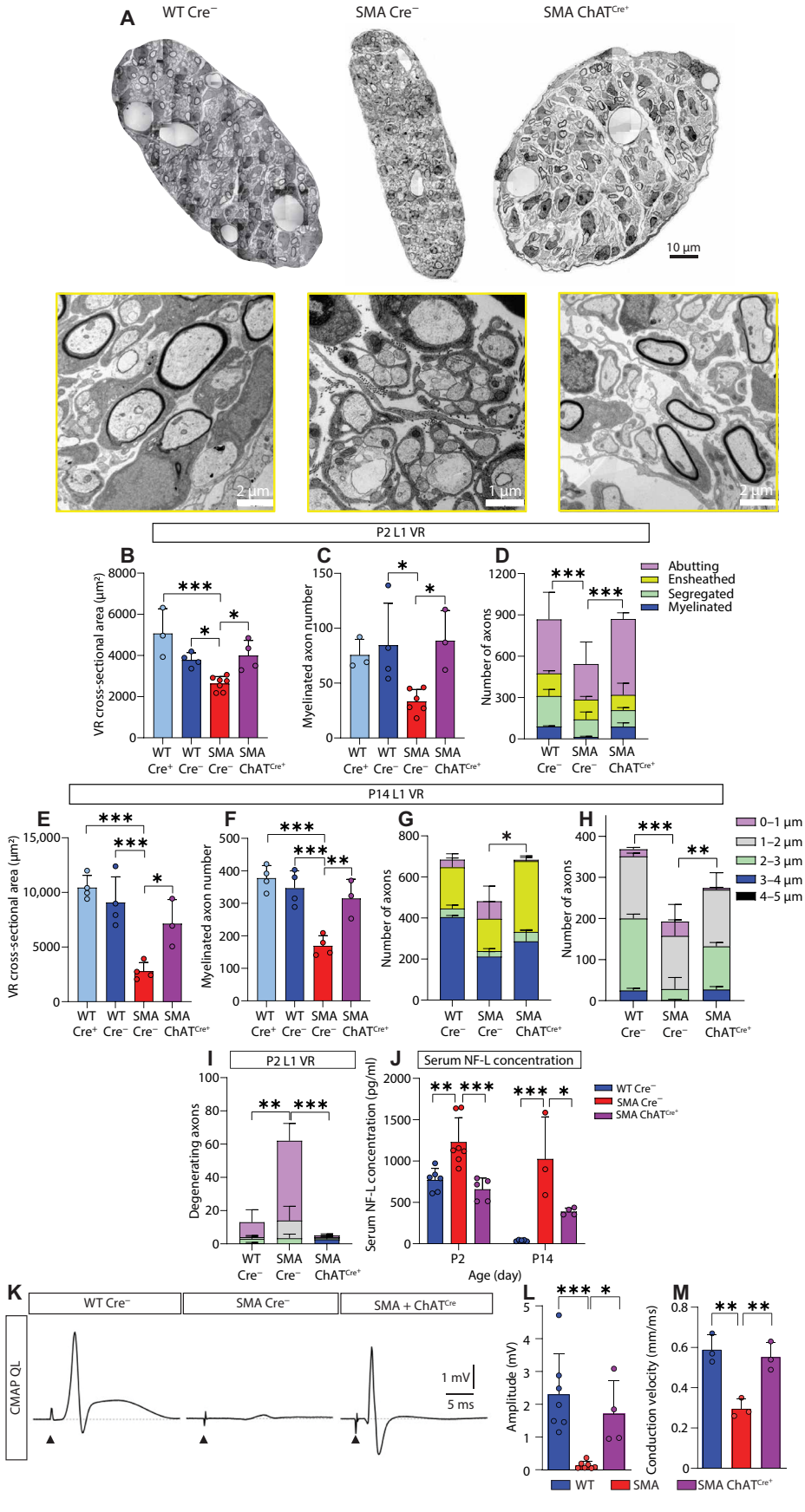

Fig. 5. Selective restoration of SMN in motor neurons restores motor axon development and function in SMA mice. (**A**) Representative reconstructed EM images and single higher-magnification images of L1 VRs in WT, SMA, and ChAT^{Cre+} SMA mice at P2. (**B** to **D**) L1 VR size ($n = 3$ to 7 each) (B), myelinated axon number ($n = 3$ to 6 each) (C), and number of axons of different categories ($n = 3$ each) (D) at P2 (* indicates significance for the myelinated axon group). (**E** to **H**) L1 VR size (E), myelinated axon number (F), number of axons of different categories (* indicates significance for ensheathed axons) (G), and diameter of axons (* indicates significance for axons of the 2-3 μm group) (H) at P14 ($n = 3$ each). (**I**) Number of degenerating axons in L1 VRs at P2 ($n = 3$ each, * indicates significance for the degenerating abutting axons). (**J**) Serum NF-L concentrations at P2 ($n = 5$ to 7 each) and P14 ($n = 3$ to 5 each). (**K**) CMAP recordings from the QL muscle after stimulation of the L1 VR at P11. Arrowheads indicate stimulus artifact. (**L** and **M**) Quantification of CMAP amplitude ($n = 4$ to 7 each) (L) and nerve CV ($n = 3$ each) (H). All data represent means and SD. Statistical analysis was performed using one-way ANOVA, corrected by Dunnett's multiple comparisons test in (B) to (D), (F) to (J), (L), and (M). Significance: $^*P \leq 0.05$; $^{**}P < 0.01$; $^{***}P < 0.001$.

SMN-C3 concentrations were detected in SMA mice treated with intraperitoneal SMN-C3 postnatally starting at P1 alone. To validate drug target engagement, we measured full-length *SMN2* transcript and protein expression in embryonic brain and spinal cord tissues from SMA mice treated starting at E9.5 or E13.5 and collected on E17.5 (fig. S10, E to K). Full-length *SMN2* transcript expression was increased by about 50%. Inductions of full-length *SMN2* transcript and SMN protein expression in P10 neural and non-neural tissues were comparable in SMA mice treated both prenatally and postnatally (starting at E9.5 or E13.5) and in SMA mice treated postnatally only (starting at P1) (fig. S10, L to W).

Mice treated with SMN-C3 starting at P1 showed increased survival as previously reported (Fig. 6A) (*35*), and their average righting time during the first 10 postnatal days was reduced by −5.87 ± 1.14 s (means ± SE) compared to the vehicle-treated SMA mice [95% confidence interval (CI): −8.10 to −3.63 s, $P < 0.001$, random effects regression analysis] (Fig. 6B). Nonetheless, SMN-C3 treatment initiated at P1 did not increase L1 VR size or myelinated axon number (Fig. 6, C to E), nor did it prevent axon loss at P14 (Fig. 6F). There was only modest improvement in radial diameter of acquired myelinated axons (Fig. 6G). In contrast, righting time was reduced by −13.63 ± 1.21 s (95% CI: −16.00 to −11.26 s, $P < 0.001$) during the first 10

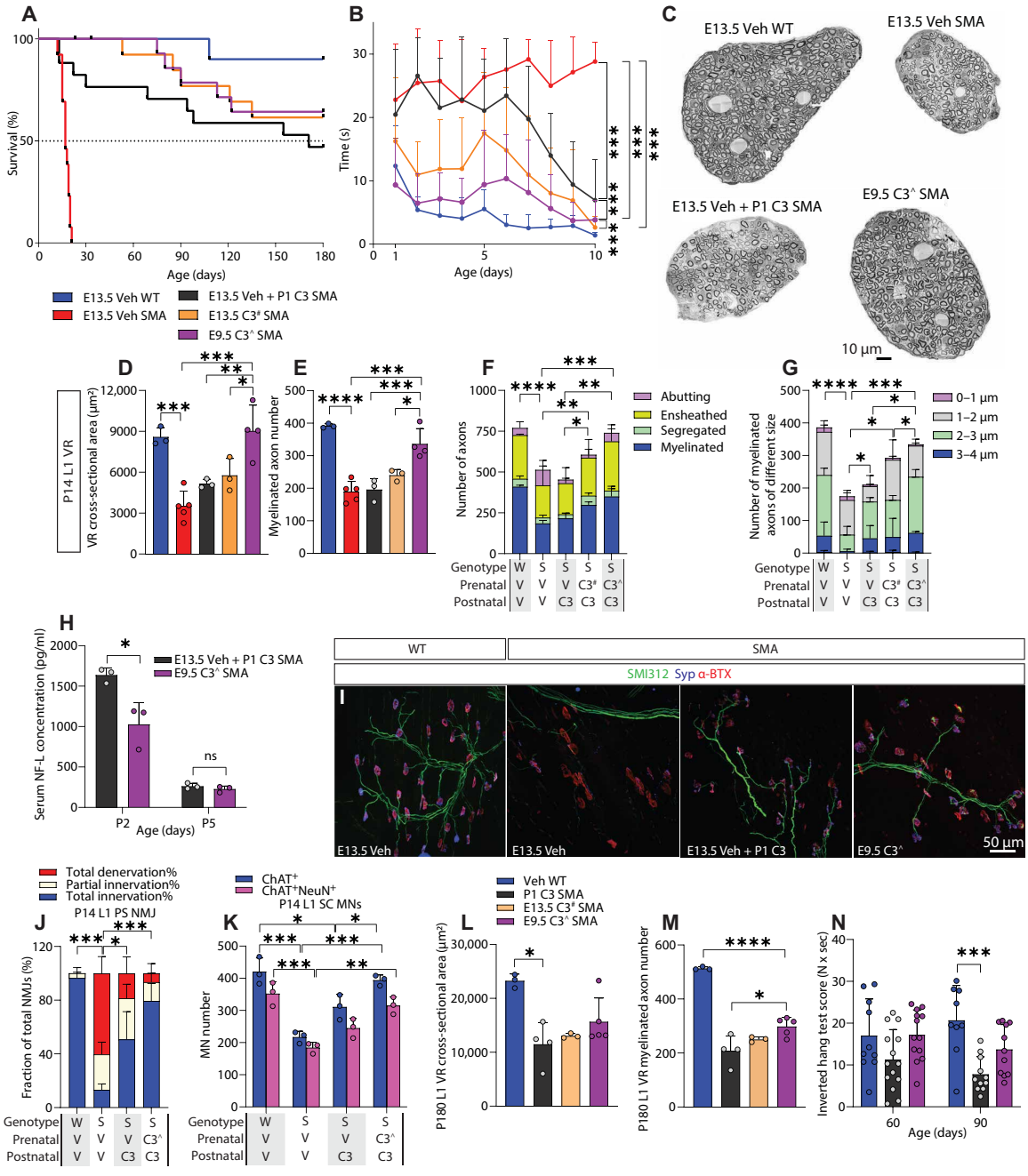

Fig. 6. Prenatal treatment with SMN-C3 prevents neonatal axon degeneration, enhances axon development, and improves motor behavior of SMA mice. (**A** and **B**) Survival (A) and righting time (B) of WT mice treated with vehicle (pre- and postnatally, $n = 10$), SMA mice treated with vehicle (pre- and postnatally, $n = 13$ to 14), SMA mice treated with vehicle prenatally and SMN-C3 postnatally ($n = 17$ to 18), SMA mice treated with SMN-C3 prenatally (starting at E13.5$^{\#}$, $n = 13$ to 14) and postnatally ($n = 14$), and SMA mice treated with SMN-C3 prenatally (starting at E9.5^) and postnatally ($n = 16$ to 19) (* represents significance between curves). (**C**) Representative EM reconstructed images of L1 VRs at P14. (**D** to **G**) L1 VR size ($n = 3$ to 5) (D), myelinated axon number ($n = 3$ to 5) (E), types of axons ($n = 3$) (F, * indicates significance of the myelinated axon category between differently treated groups.), and myelinated axon diameter ($n = 3$) (G, * indicates significance of myelinated axons between 2-3 µm in diameter between the differently treated groups) at P14. (**H**) Serum NF-L concentrations at P2 or P5 ($n = 3$ each). (**I**) Confocal images of P14 L1 PS muscle NMJs stained with SMI312 (blue), synaptophysin (purple), and α-BTX (red). (**J**) NMJ innervation in L1 PS muscle at P14 ($n = 3$ each, * indicates significance of the total innervation% category between differently treated groups). (**K**) MN number in the L1 spinal cord segment at P14 ($n = 3$ each). (**L** and **M**) L1 VR size (E) and myelinated axon number (F) at P180 ($n = 3$ to 5). (**N**) Hang time test at P60 and P90 ($n = 10$ to 14). W, WT; S, SMA; V, vehicle; C3$^{\#}$, SMN-C3 starting at E13.5; C3^, SMN-C3 starting at E9.5. In (A), statistical analysis was performed using log-rank test. In all other graphs, data represent means and SD. Statistical analysis was performed in (B) using random effects regression test; in (D) to (G) and (J) to (N) using one-way ANOVA with Tukey's post hoc test; and in (H) using unpaired t test. Significance: *$P \leq 0.05$; **$P < 0.01$; ***$P < 0.001$, ****$P < 0.0001$.

postnatal days when SMN-C3 was started at E13.5 and −18.34 ± 1.17 s (95% CI: −20.64 to −16.04 s, $P < 0.001$) when SMN-C3 treatment was started at E9.5 compared to vehicle-treated SMA mice (Fig. 6B). Fetal initiation of treatment also increased VR size, acquisition of myelinated axons, and axon radial growth (Fig. 6, C to G). Initiation of SMN-C3 at E9.5 also prevented proximal L1 axon loss in SMA mice at P14 (Fig. 6F) and reduced serum NF-L concentrations at P2 compared to SMA mice initiating SMN-C3 treatment at P1 (Fig. 6H). Improvements in axon development and maintenance caused by fetal initiation of treatment at E9.5 was also associated with maintenance of L1 PS innervation (Fig. 6, I to J) and MN soma number (Fig. 6K) at P14, and less deterioration of VR histology (Fig. 6, L and M) and motor function (Fig. 6N) in adult mice. To confirm that histological improvements correlated with changes in function, we examined motor axon electrophysiology in treated mice at P11. SMA mice receiving SMN-C3 starting at P1 showed no improvement in QL CMAP amplitude or axonal CV (Fig. 7, A to C) compared to vehicle-treated SMA mice. In contrast, in SMA mice receiving SMN-C3 treatment starting at E9.5, there was improvement of CMAP amplitudes and near-complete normalization of CV (Fig. 7, A to C). Administration of a second splice switching molecule with further optimized pharmaceutical properties SMN-C8 [compound 5 in (*10*)] to pregnant dams throughout gestation by daily oral dosing also resulted in robust improvements in neonatal motor behavior compared to mice treated with SMN-C8 postnatally alone (fig. S11). Together, these data indicate that increase in SMN expression during embryonic development by treatment with small-molecule *SMN2* splice modifiers results in enhanced motor unit development, motor axon function, and short- and long-term motor behavior in SMA mice.

DISCUSSION

Our pathological characterizations of tissue from patients with Type 1 SMA integrated with longitudinal genetic, histological, electrophysiological, and biochemical studies of severe SMA model mice reveal that restricted embryonic motor axon radial growth and impaired Schwann cell ensheathment are initial cellular features of severe SMA. Those axons that lag the most in fetal radial growth are subject to precipitous degeneration postnatally. The rapidity of this irreversible motor unit loss provides biological insight into why early initiation of SMN induction therapy is associated with the greatest treatment effect in patients with SMA. However, our findings also suggest that the optimal timing of SMN induction therapeutics may precede the onset of overt axonal degeneration. Improved outcomes of SMA treated with SMN-C3 earlier in gestation may point to a restricted temporal window for remediating early disturbances of motor axon development. Those SMA motor axons that grow sufficiently to enable myelination are relatively resistant to degeneration in the early postnatal period, but are nonetheless smaller, electrophysiologically abnormal, and vulnerable to further slow degeneration. This disrupted developmental cascade, with its associated rapid loss of the most immature axons followed later by slow degeneration of more mature axons, offers potential explanation for the heretofore enigmatic and unusual clinical disease course of patients with severe infantile SMA. Together, these studies underscore the importance of early initiation of treatment of infants with Type 1 SMA, supply a rationale for exploring fetal treatment of severe patients, and suggest an opportunity for development of better combination therapeutics.

Radial growth of axons is the first step that enables Schwann cell ensheathment and later segregation and myelination. In mice, Schwann cells first ensheath axons beginning at E12.5, 1:1 segregation starts at ~E17.5, and the first compact myelin sheaths are formed at P1 with myelination complete by ~P10 (fig. S1). This developmental sequence is slower in humans, but largely completed in utero. Ensheathment begins at 10 to 11 weeks' gestation, the first axons are myelinated at 16 weeks, and myelination is completed by birth with continued radial growth and myelin thickening occurring postnatally (*21*, *22*). The abundant, abutting axons we observed in human postnatal SMA, but not control VRs, are likely arrested at fetal stages of development. They are unlikely to represent miswired sensory or autonomic axons because these would be anticipated to be ensheathed within Remak bundles. Whereas they could be aberrantly branched or defasciculated motor axons reminiscent of those that arise during motor axon outgrowth in a zebrafish model of SMA (*36*), the normal total number of L1 VR axons and intact NMJ innervation in SMAΔ7 mice at E13.5 argues against this possibility. Although motor axon developmental abnormalities are evident in both patients with

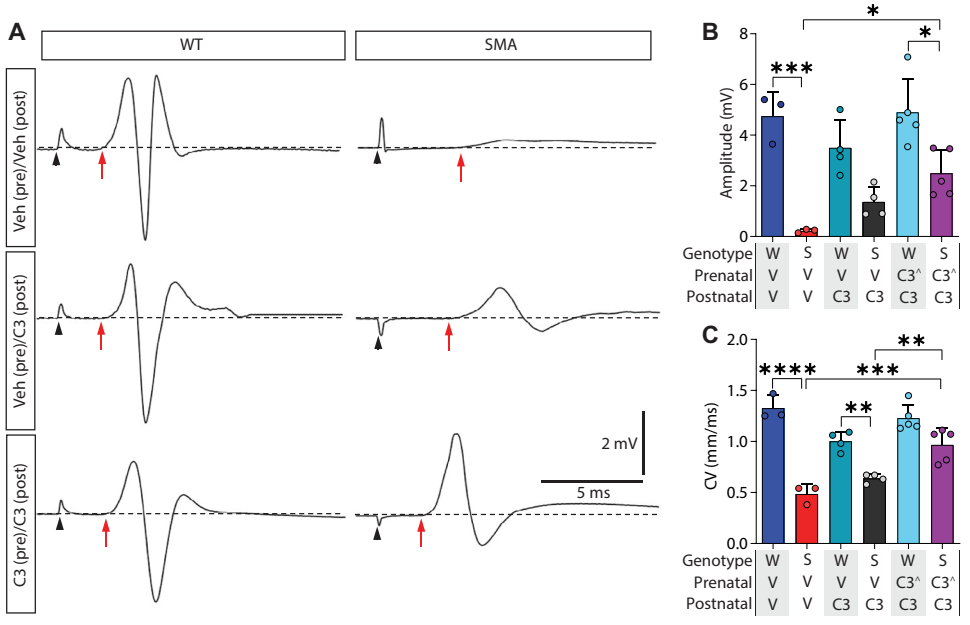

Fig. 7. Prenatal treatment with SMN-C3 improves motor axon function. (**A**) CMAP recordings from the QL muscle after L1 VR stimulation at P11. Red arrows indicate shortest latency of CMAP response. Black arrowheads indicate stimulus artifact. (**B** and **C**) Quantification of CMAP amplitudes ($n = 3$ to 5) (B) and nerve CVs ($n = 3$ to 5) (C) from WT (W) and SMA (S) mice receiving vehicle (V) or SMN-C3 treatment starting prenatally at E9.5 (C3^) or postnatally at P1. In (B) and (C), statistical analysis was performed using one-way ANOVA with Tukey's post hoc test. Significance: *$P \leq 0.05$; **$P < 0.01$; ***$P < 0.001$, ****$P < 0.0001$.

infantile SMA and severe SMA model mice, they are substantially more severe in patients as indicated by the proportion of affected axons, the magnitude of radial growth deficits, and the topographical extent. SMN protein expression is particularly high in human spinal cord during gestation (*37*), consistent with a requirement for SMN during the period when axon radial growth and Schwann cell ensheathment occur in humans.

Bi-directional signaling between axons and their investing Schwann cells during development is mediated by specialized molecules located in the opposing axolemma and adaxonal Schwann cell membranes (*14*, *15*). A previous study demonstrated that overexpression of SMN in myelinating Schwann cells in SMA mice does not extend mouse survival or prevent loss of MNs, but does result in increased myelin thickness and improved righting time (*38*). When examining the earliest stages of axonal development in this study, we demonstrate that myelination proceeds normally when axons expand radially beyond the common mammalian threshold diameter of about 1 μm in patients with SMA and SMA mice. Furthermore, genetically targeted restoration of SMN expression to MNs resulted in increased radial axonal growth and myelination with near normalization of motor axon electrophysiology, whereas restoration in Schwann cells showed no benefit and restoration in muscle resulted in only modest increases of axon diameter. These data argue that SMN deficiency in MNs is the key determinant of initial diminished radial axonal growth, which subsequently impairs axon–Schwann cell developmental interactions, and suggests that effective early SMN induction in this cell type is required for optimal therapeutic efficacy.

Impaired radial growth is evident in most SMA motor axons to a variable degree but differs according to specific topographic vulnerability within and between humans and the SMAΔ7 mouse. Wherever axonal maturation is most impaired, however, there is preferential postnatal degeneration of the smallest and most developmentally delayed axons. Whether this selective degeneration is a consequence of relative diminished SMN expression, a downstream consequence of altered trophic support from investing Schwann cells and muscle, or some combination of these two is unknown. Schwann cell trophic support is necessary for maintenance of developing motor axons and their soma. Neuregulin 1 type III (NRG1-III), which is expressed on axons, interacts with ErbB2/3 receptors on Schwann cells and is essential for axon ensheathment and myelination (*39*, *40*). In ErbB2-, ErbB3-, or NRG1-III–null mice, projecting MN axons form NMJs at E15.5, but precipitous loss of motor axons and MN somata occurs by E18.5 (*41*–*43*). Development of the embryonic motor unit involves interdependence between axons and investing Schwann cells and between axons and innervated muscle (*44*, *45*) and may account for the parallel early loss of both motor axons and MN somata in SMA mice during the first two postnatal days.

The natural history of patients with infantile onset SMA is not characteristic of most neurodegenerative disorders. Instead, infants with SMA Type 1 often demonstrate an initial decline followed by a plateau (*4*, *5*). In one natural history study, onset of weakness occurred within 1 to 2 months of birth with ~50% reduction of motor function scores by 3 to 4 months and less rapid declines thereafter (*5*). Longitudinal electrophysiologically derived estimates of motor unit number in a small number of infants with Type 1 SMA found a precipitous decline to very low number within 1 to 2 months with little subsequent change (*46*). Our investigations demonstrating a bimodal population of SMA motor units provide cellular insights into these observations. The early and abrupt clinical decline of patients may be caused by the rapid degeneration of the most immature SMA motor axons. Because these axons are extremely small in diameter and not myelinated, they are detectable only with EM and may be difficult to record electrophysiologically with standard surface stimulation and recording techniques. The SMA axons that have expanded radially to enable myelination degenerate more slowly, which may account for the later, slowly progressive phase of disease. In our study of patients with SMA, a small fraction of these myelinated axons were degenerating in VRs, in contrast to the ~20 to 40% rate of degeneration in autopsy studies of amyotrophic lateral sclerosis, a demonstrably progressive MN degenerative disorder (*47*, *48*). We observed reductions of total myelinated axon number, low rates of degeneration of these myelinated axons, and abundant hypotrophic myofibers in one to two patients with Type 2 SMA, suggesting that a proportion of Type 2 SMA axons are also developmentally arrested and degenerate early, although not in sufficient numbers to cause severe weakness in the first months of life.

Blood NF concentrations are being developed as a biomarker of neurodegeneration in multiple neurodegenerative disorders (*28*) including SMA (*49*). Unlike many neurodegenerative diseases in which NFs remain elevated or increased during the disease course, blood pNF-H concentrations are most elevated in the youngest patients with SMA Type 1, with two copies of *SMN2*, during the limited days or weeks before manifesting symptomatic weakness (*12*, *49*). Species differences in MN developmental NF expression patterns, especially with respect to onset of manifest weakness in SMA, are likely important. In our study of SMA mice, the initial, neonatal spike of NF-L release at P1 and P2 was not associated with pNF-H release, whereas at late time points (P3 to P14), both NF subtypes were elevated. This early exclusive release of NF-L parallels our data demonstrating that the small, abutting axons, which express NF-L exclusively, degenerate neonatally in SMA mice. The timing of early developmental MN NF-L and pNF-H expression in humans is not known, but formation of compact myelin is known to be associated with increased radial diameter partly attributable to expression of all three NF subunits (*50*). In this study of human autopsy cases, all patients with SMA showed signs of both small and, to a lesser degree, large, myelinated axon degeneration. The point at which neurodegeneration of the most vulnerable axons first begins in patients with severe SMA thus remains unknown. A priority for ongoing work is to determine the normal developmental patterns of NF-L and pNF-H and their perturbations in the serum of patients with SMA, including assessment of prenatal and neonatal time points to determine when neurodegenerative disease activity first begins in patients with different disease severities.

Further advances in electrophysiology of infants might also provide an opportunity for monitoring SMA disease progression and response to therapeutics. During the first 2 weeks of postnatal development in WT mice, a 3.8-fold increase in CMAP amplitude and a 4.4-fold increase of CV resulted from the normal increase of L1 VR myelinated axon numbers (from 30 to 378 axons) and their diameters (from 1.9 to 2.4 μm). Postnatal maturation of peripheral axon physiology also occurs in humans with a doubling of CMAP amplitude and CV between birth and 3 to 5 years of life (*51*, *52*). Our studies of SMA mice demonstrate that L1 VR reduced CMAP amplitudes at birth, reminiscent of the reduced CMAP amplitudes often present even in very young Type 1 patients with SMA. In

contrast, the relatively spared SMAΔ7 mouse L5 VRs attain a normal number of myelinated axons at P1 that generate a normal CMAP amplitude confirming that topographic variations in neurophysiology track with the anatomic changes. Our electrophysiological studies also showed reductions of CV in SMA compared to WT mice. Modest slowing of motor CV has been reported in patients with SMA (*53*, *54*), which was generally attributed to degeneration of the largest, most rapidly conducting axons. Our data suggest that conduction slowing in SMA mice is at least initially caused by impaired radial growth, rather than the selective later loss of the largest axons. If similar phenomena underlie motor nerve conduction slowing in humans, then a therapeutic implication is the potential opportunity to increase radial diameter and function of those motor axons that have not succumbed to degeneration.

Clinical trials of nusinersen and onasemnogene abeparvovec have demonstrated that earlier initiation of treatment is associated with substantially greater efficacy (*7*, *9*, *12*). These data have prompted development and institution of newborn screening (NBS) programs for SMA in many countries including the United States, so that these expensive therapies can be given early when the treatment effect is greatest. Although rapid initiation of therapy undoubtedly improved outcomes, half of the patients with two copies of *SMN2* identified by NBS in Australia and Germany were already overtly symptomatic at the median time of treatment at 26.5 and 24 days, respectively (*55*, *56*). Our study highlights the rapidity of degeneration of the most immature and vulnerable axons soon after birth in SMA mice and implies that treatment delays of days or weeks in humans could substantially affect long-term clinical outcomes. The specialized and expensive nature of these treatments requires careful consideration of procedures and infrastructures to enable initiation of treatment as soon after birth as possible. One strategy might be to increase use of maternal carrier screening and, if appropriate, fetal genetic testing such that insurance approval can be obtained before birth.

Given the severe axon developmental defects seen in our youngest SMA cases, postnatal treatment alone may be insufficient to normalize outcomes for all of those infants with early infantile onset of weakness, as well as a rarer group of infants manifesting weakness at the time of birth (Type 0 SMA). Our studies demonstrate that early embryonic treatment is required in severe SMA mice not only to prevent loss of the most immature axons but also to maximize maturation of surviving axons. In mice, we demonstrate that an analog of the orally bioavailable *SMN2* splice switching drug risdiplam can be delivered safely to pregnant dams with sufficient bioavailability in SMA fetuses to improve axonal development, electrophysiology, and motor behavior. Although prenatal *SMN* gene replacement treatment of embryonic mice was recently shown to improve outcomes of surviving SMA mice, fetal intracerebroventricular injection was also associated with in utero toxicity with only ~41 to 44% of SMA embryos surviving to birth (*57*). Further investigations will be needed to determine whether small-molecule splice modifiers or other SMN induction therapeutics are indicated, safe, and efficacious when used for in utero treatment of humans. Future studies are also needed to define the molecular mechanisms downstream of SMN deficiency that underlie constrained developmental axonal radial growth, impaired axon–Schwann cell relationships, and axonal death. Early antagonism of axonal self-destruction pathways (*58*), for example, might provide additional time needed for SMN induction therapeutics to have maximal effect. The impaired developmental sequence identified here offers potential insights into the pathogenesis of severe infantile SMA that may ultimately lead to previously unexplored combination therapies.

As our human studies rely solely on postmortem autopsy tissues, our histologic assessments are limited to those with end-stage disease and may be complicated by pre- and postmortem confounders. We attempted to minimize these effects by characterizing a large series of SMA cases and age-matched controls. Future autopsy studies of fetal SMA cases and more mildly affected, later-onset patients with SMA will further our understanding of the spectrum of SMA disease pathology. As longitudinal morphological assessment of SMA motor axon abnormalities is not possible in living patients, we pursued histochemical, ultrastructural, and electrophysiological investigations at multiple time points in a mouse model of SMA. The use of a genetic mouse model may introduce potential species or strain-specific confounders not relevant to human SMA, and thus, pharmacological studies in SMA mice are not necessarily predictive of outcomes in human patients. Nonetheless, the shared delayed axon development features in both human patients and SMA mice do strongly suggest that abnormalities of motor axon development begin in utero in infantile onset patients and are associated with rapid postnatal degeneration. Although our therapeutic intervention studies in SMA mice show improved outcomes with treatment initiated in utero, our present ability to predict outcomes of SMA fetuses based on present genetic investigations is at best rudimentary. Improved predictors will be needed before fetal-based treatment trials can be contemplated, and this emphasizes the need for continued development of novel biomarkers based on improved understanding of disease pathobiology.

MATERIALS AND METHODS

Study design

The objective was to use human postmortem tissues and SMA model mice to characterize the earliest disease pathologies that dictate the timing of therapeutic intervention. Expedited autopsies were conducted under parental- or patient-informed consent in strict observance of the legal and institutional ethical regulations. Tissues from patients with SMA and age-matched controls with a short postmortem interval were included. Breeding and treatment of mice were performed in accordance with National Institutes of Health guidelines and protocols approved by Institutional Animal Care and Use Committees (IACUCs) at John Hopkins University School of Medicine and Columbia University. SMAΔ7 (JAX#00525) mice underwent histological, electrophysiological, and biochemical analyses. They were treated with the *SMN2* splicing modifier drugs (SMN-C3 and C8) or vehicle. Sample size was determined by previous experience, preliminary data, and power calculations. The mice were randomized to treatment group, and the investigators who assessed the behavioral, histological, biochemical, and electrophysiological outcomes were blinded to the treatment group. Please see Supplementary Materials and Methods for further details.

Statistical analysis

Results are expressed as median or means ± SD from at least three independent samples per group. Differences between two groups were analyzed by a two-tailed unpaired Student's *t* test or Mann-Whitney for nonparametric analysis, where appropriate. Changes over developmental time were analyzed using linear regression analyses to determine slopes and differences in slopes. Differences among three or more groups were analyzed by one-way analysis of variance (ANOVA)

using Tukey's post hoc correction or multiple comparisons corrected by Dunnett's test using GraphPad Prism 8. Behavioral data from three or more groups were compared using random-effect linear regression test by an independent statistician. Survival curves were compared using log-rank test.

SUPPLEMENTARY MATERIALS

stm.sciencemag.org/cgi/content/full/13/578/eabb6871/DC1
Materials and Methods
Fig. S1. Schematic of normal peripheral axon development in rodents.
Fig. S2. Severe myofiber hypotrophy in iliopsoas and intercostal, but not diaphragm muscle in patients with SMA.
Fig. S3. Compared to VRs, axons are relatively preserved in DRs and phrenic nerves of patients with SMA.
Fig. S4. Intramuscular axons and MNs are also abnormal in patients with SMA.
Fig. S5. Thoracic VRs are similarly affected as L1 VRs whereas DRs are spared in SMA mice.
Fig. S6. Progressive loss of NMJ innervation and MNs in SMA mice accompanied by arrest of myofiber growth.
Fig. S7. Increased latency of CMAP response in SMA mice is due to reduced nerve CV and not NMJ synaptic delay.
Fig. S8. Cell-specific increase of SMN expression in Schwann cells does not improve the survival or motor behavior of SMA mice.
Fig. S9. Cell-specific increase of SMN expression in Schwann cells or muscles results in little improvement of motor axon survival or development.
Fig. S10. Dosing of SMN-C3 to pregnant dams and postnatal mice increases SMN expression in neural tissues.
Fig. S11. Oral dosing of SMN-C8 to pregnant dams throughout gestation improves motor behavior of SMA mice.
Table S1. SMA and age-matched control autopsy cases.
Table S2. Antibody list.
Data file S1. Raw data (provided as separate Excel file).
References (*59*–*63*)

View/request a protocol for this paper from *Bio-protocol*.

REFERENCES AND NOTES

1. S. Lefebvre, L. Burglen, S. Reboullet, O. Clermont, P. Burlet, L. Viollet, B. Benichou, C. Cruaud, P. Millasseau, M. Zeviani, D. Le Paslier, J. Frézal, D. Cohen, J. Weissenbach, A. Munnich, J. Melki, Identification and characterization of a spinal muscular atrophy-determining gene. *Cell* **80**, 155–165 (1995).
2. C. L. Lorson, E. Hahnen, E. J. Androphy, B. Wirth, A single nucleotide in the SMN gene regulates splicing and is responsible for spinal muscular atrophy. *Proc. Natl. Acad. Sci. U.S.A.* **96**, 6307–6311 (1999).
3. U. R. Monani, C. L. Lorson, D. W. Parsons, T. W. Prior, E. J. Androphy, A. H. Burghes, J. D. McPherson, A single nucleotide difference that alters splicing patterns distinguishes the SMA gene SMN1 from the copy gene SMN2. *Hum. Mol. Genet.* **8**, 1177–1183 (1999).
4. R. S. Finkel, M. P. McDermott, P. Kaufmann, B. T. Darras, W. K. Chung, D. M. Sproule, P. B. Kang, A. R. Foley, M. L. Yang, W. B. Martens, M. Oskoui, A. M. Glanzman, J. Flickinger, J. Montes, S. Dunaway, J. O'Hagen, J. Quigley, S. Riley, M. Benton, P. A. Ryan, M. Montgomery, J. Marra, C. Gooch, D. C. De Vivo, Observational study of spinal muscular atrophy type I and implications for clinical trials. *Neurology* **83**, 810–817 (2014).
5. S. J. Kolb, C. S. Coffey, J. W. Yankey, K. Krosschell, W. D. Arnold, S. B. Rutkove, K. J. Swoboda, S. P. Reyna, A. Sakonju, B. T. Darras, R. Shell, N. Kuntz, D. Castro, J. Parsons, A. M. Connolly, C. A. Chiriboga, C. McDonald, W. B. Burnette, K. Werner, M. Thangarajh, P. B. Shieh, E. Finanger, M. E. Cudkowicz, M. M. McGovern, D. E. McNeil, R. Finkel, S. T. Iannaccone, E. Kaye, A. Kingsley, S. R. Renusch, V. L. McGovern, X. Wang, P. G. Zaworski, T. W. Prior, A. H. M. Burghes, A. Bartlett, J. T. Kissel; NeuroNEXT Clinical Trial Network on behalf of the NN101 SMA Biomarker Investigators, Natural history of infantile-onset spinal muscular atrophy. *Ann. Neurol.* **82**, 883–891 (2017).
6. D. W. Parsons, P. E. McAndrew, S. T. Iannaccone, J. R. Mendell, A. H. Burghes, T. W. Prior, Intragenic telSMN mutations: Frequency, distribution, evidence of a founder effect, and modification of the spinal muscular atrophy phenotype by cenSMN copy number. *Am. J. Hum. Genet.* **63**, 1712–1723 (1998).
7. R. S. Finkel, E. Mercuri, B. T. Darras, A. M. Connolly, N. L. Kuntz, J. Kirschner, C. A. Chiriboga, K. Saito, L. Servais, E. Tizzano, H. Topaloglu, M. Tulinius, J. Montes, A. M. Glanzman, K. Bishop, Z. J. Zhong, S. Gheuens, C. F. Bennett, E. Schneider, W. Farwell, D. C. De Vivo; ENDEAR Study Group, Nusinersen versus sham control in infantile-onset spinal muscular atrophy. *N. Engl. J. Med.* **377**, 1723–1732 (2017).
8. E. Mercuri, B. T. Darras, C. A. Chiriboga, J. W. Day, C. Campbell, A. M. Connolly, S. T. Iannaccone, J. Kirschner, N. L. Kuntz, K. Saito, P. B. Shieh, M. Tulinius, E. S. Mazzone, J. Montes, K. M. Bishop, Q. Yang, R. Foster, S. Gheuens, C. F. Bennett, W. Farwell, E. Schneider, D. C. De Vivo, R. S. Finkel; CHERISH Study Group, Nusinersen versus sham control in later-onset spinal muscular atrophy. *N. Engl. J. Med.* **378**, 625–635 (2018).
9. J. R. Mendell, S. Al-Zaidy, R. Shell, W. D. Arnold, L. R. Rodino-Klapac, T. W. Prior, L. Lowes, L. Alfano, K. Berry, K. Church, J. T. Kissel, S. Nagendran, J. L'Italien, D. M. Sproule, C. Wells, J. A. Cardenas, M. D. Heitzer, A. Kaspar, S. Corcoran, L. Braun, S. Likhite, C. Miranda, K. Meyer, K. D. Foust, A. H. M. Burghes, B. K. Kaspar, Single-dose gene-replacement therapy for spinal muscular atrophy. *N. Engl. J. Med.* **377**, 1713–1722 (2017).
10. H. Ratni, M. Ebeling, J. Baird, S. Bendels, J. Bylund, K. S. Chen, N. Denk, Z. Feng, L. Green, M. Guerard, P. Jablonski, B. Jacobsen, O. Khwaja, H. Kletzl, C. P. Ko, S. Kustermann, A. Marquet, F. Metzger, B. Mueller, N. A. Naryshkin, S. V. Paushkin, E. Pinard, A. Poirier, M. Reutlinger, M. Weetall, A. Zeller, X. Zhao, L. Mueller, Discovery of risdiplam, a selective survival of motor neuron-2 (SMN2) gene splicing modifier for the treatment of spinal muscular atrophy (SMA). *J. Med. Chem.* **61**, 6501–6517 (2018).
11. C. J. Sumner, T. O. Crawford, Two breakthrough gene-targeted treatments for spinal muscular atrophy: Challenges remain. *J. Clin. Invest.* **128**, 3219–3227 (2018).
12. D. C. De Vivo, E. Bertini, K. J. Swoboda, W. L. Hwu, T. O. Crawford, R. S. Finkel, J. Kirschner, N. L. Kuntz, J. A. Parsons, M. M. Ryan, R. J. Butterfield, H. Topaloglu, T. Ben-Omran, V. A. Sansone, Y. J. Jong, F. Shu, J. F. Staropoli, D. Kerr, A. W. Sandrock, C. Stebbins, M. Petrillo, G. Braley, K. Johnson, R. Foster, S. Gheuens, I. Bhan, S. P. Reyna, S. Fradette, W. Farwell; NURTURE Study Group, Nusinersen initiated in infants during the presymptomatic stage of spinal muscular atrophy: Interim efficacy and safety results from the Phase 2 NURTURE study. *Neuromuscul. Disord.* **29**, 842–856 (2019).
13. G. Werdnig, Zwei frühinfantile hereditäre fälle von progressiver muskelatrophie unter dem bilde der dystrophie, aber anf neurotischer grundlage. *Arch. für Psychiatr. Nervenkrankh.* **22**, 437–480 (1891).
14. M. L. Feltri, Y. Poitelon, S. C. Previtali, How Schwann cells sort axons: New concepts. *Neuroscientist* **22**, 252–265 (2016).
15. R. Fledrich, T. Kungl, K. A. Nave, R. M. Stassart, Axo-glial interdependence in peripheral nerve development. *Development* **146**, dev151704 (2019).
16. W. C. Robertson Jr., Y. Kawamura, P. J. Dyck, Morphometric study of motoneurons in congenital nemaline myopathy and Werdnig-Hoffmann disease. *Neurology* **28**, 1057–1061 (1978).
17. J. H. Skene, R. D. Jacobson, G. J. Snipes, C. B. McGuire, J. J. Norden, J. A. Freeman, A protein induced during nerve growth (GAP-43) is a major component of growth-cone membranes. *Science* **233**, 783–786 (1986).
18. R. Curtis, H. J. Stewart, S. M. Hall, G. P. Wilkin, R. Mirsky, K. R. Jessen, GAP-43 is expressed by nonmyelin-forming Schwann cells of the peripheral nervous system. *J. Cell Biol.* **116**, 1455–1464 (1992).
19. M. J. Carden, J. Q. Trojanowski, W. W. Schlaepfer, V. M. Lee, Two-stage expression of neurofilament polypeptides during rat neurogenesis with early establishment of adult phosphorylation patterns. *J. Neurosci.* **7**, 3489–3504 (1987).
20. H. Y. Ko, Y. B. Shin, H. J. Sohn, J. H. Chang, Y. H. Ahn, Y. H. Ha, Unmyelinated fibers in human spinal ventral roots: C4 to S2. *Spinal Cord* **47**, 286–289 (2009).
21. H. J. Gamble, Further electron microscope studies of human foetal peripheral nerves. *J. Anat.* **100**, 487–502 (1966).
22. I. Niebrój-Dobosz, A. Fidziańska, J. Rafałwska, E. Sawicka, Correlative biochemical and morphological studies of myelination in human ontogenesis. II. Myelination of the nerve roots. *Acta Neuropathol* **49**, 153–158 (1980).
23. A. Fidzianska, I. Hausmanowa-Petrusewicz, Clinical features of infantile and juvenile spinal muscular atrophy, in *Progressive Spinal Muscular Atrophies,* I. Gamstorp, H. B. Sarnat, Eds. (Raven Press, 1984), vol. International Review of Child Neurology Series, pp. 31–42.
24. G. Z. Mentis, W. Liu, D. Blivis, E. Drobac, M. E. Crowder, L. Kong, F. J. Alvarez, C. J. Sumner, M. J. O'Donovan, Early functional impairment of sensory-motor connectivity in a mouse model of spinal muscular atrophy. *Neuron* **10**, 453–467 (2011).
25. T. J. Biscoe, S. M. Nickels, C. A. Stirling, Numbers and sizes of nerve fibres in mouse spinal roots. *Q. J. Exp. Physiol.* **67**, 473–494 (1982).
26. N. Bogduk, A. S. Wilson, W. Tynan, The human lumbar dorsal rami. *J. Anat.* **134**, 383–397 (1982).
27. N. Stifani, Motor neurons and the generation of spinal motor neuron diversity. *Front. Cell. Neurosci.* **8**, 293 (2014).
28. M. Khalil, C. E. Teunissen, M. Otto, F. Piehl, M. P. Sormani, T. Gattringer, C. Barro, L. Kappos, M. Comabella, F. Fazekas, A. Petzold, K. Blennow, H. Zetterberg, J. Kuhle, Neurofilaments as biomarkers in neurological disorders. *Nat. Rev. Neurol.* **14**, 577–589 (2018).
29. E. V. Fletcher, C. M. Simon, J. G. Pagiazitis, J. I. Chalif, A. Vukojicic, E. Drobac, X. Wang, G. Z. Mentis, Reduced sensory synaptic excitation impairs motor neuron function via Kv2.1 in spinal muscular atrophy. *Nat. Neurosci.* **20**, 905–916 (2017).
30. C. M. Lutz, S. Kariya, S. Patruni, M. A. Osborne, D. Liu, C. E. Henderson, D. K. Li, L. Pellizzoni, J. Rojas, D. M. Valenzuela, A. J. Murphy, M. L. Winberg, U. R. Monani, Postsymptomatic restoration of SMN rescues the disease phenotype in a mouse model of severe spinal muscular atrophy. *J. Clin. Invest.* **121**, 3029–3041 (2011).

31. P. E. Phelps, R. P. Barber, J. E. Vaughn, Embryonic development of choline acetyltransferase in thoracic spinal motor neurons: Somatic and autonomic neurons may be derived from a common cellular group. *J. Comp. Neurol.* **307**, 77–86 (1991).
32. E. Parmantier, B. Lynn, D. Lawson, M. Turmaine, S. S. Namini, L. Chakrabarti, A. P. McMahon, K. R. Jessen, R. Mirsky, Schwann cell-derived Desert hedgehog controls the development of peripheral nerve sheaths. *Neuron* **23**, 713–724 (1999).
33. O. Kanisicak, J. J. Mendez, S. Yamamoto, M. Yamamoto, D. J. Goldhamer, Progenitors of skeletal muscle satellite cells express the muscle determination gene, MyoD. *Dev. Biol.* **332**, 131–141 (2009).
34. T. L. Martinez, L. Kong, X. Wang, M. A. Osborne, M. E. Crowder, J. P. Van Meerbeke, X. Xu, C. Davis, J. Wooley, D. J. Goldhamer, C. M. Lutz, M. M. Rich, C. J. Sumner, Survival motor neuron protein in motor neurons determines synaptic integrity in spinal muscular atrophy. *J. Neurosci.* **32**, 8703–8715 (2012).
35. N. A. Naryshkin, M. Weetall, A. Dakka, J. Narasimhan, X. Zhao, Z. Feng, K. K. Ling, G. M. Karp, H. Qi, M. G. Woll, G. Chen, N. Zhang, V. Gabbeta, P. Vazirani, A. Bhattacharyya, B. Furia, N. Risher, J. Sheedy, R. Kong, J. Ma, A. Turpoff, C. S. Lee, X. Zhang, Y. C. Moon, P. Trifillis, E. M. Welch, J. M. Colacino, J. Babiak, N. G. Almstead, S. W. Peltz, L. A. Eng, K. S. Chen, J. L. Mull, M. S. Lynes, L. L. Rubin, P. Fontoura, L. Santarelli, D. Haehnke, K. D. McCarthy, R. Schmucki, M. Ebeling, M. Sivaramakrishnan, C. P. Ko, S. V. Paushkin, H. Ratni, I. Gerlach, A. Ghosh, F. Metzger, Motor neuron disease. SMN2 splicing modifiers improve motor function and longevity in mice with spinal muscular atrophy. *Science* **345**, 688–693 (2014).
36. T. Hao le, P. Q. Duy, J. D. Jontes, M. Wolman, M. Granato, C. E. Beattie, Temporal requirement for SMN in motoneuron development. *Hum. Mol. Genet.* **22**, 2612–2625 (2013).
37. D. M. Ramos, C. d'Ydewalle, V. Gabbeta, A. Dakka, S. K. Klein, D. A. Norris, J. Matson, S. J. Taylor, P. G. Zaworski, T. W. Prior, P. J. Snyder, D. Valdivia, C. L. Hatem, I. Waters, N. Gupte, K. J. Swoboda, F. Rigo, C. F. Bennett, N. Naryshkin, S. Paushkin, T. O. Crawford, C. J. Sumner, Age-dependent SMN expression in disease-relevant tissue and implications for SMA treatment. *J. Clin. Invest.* **129**, 4817–4831 (2019).
38. G. Hunter, R. A. Powis, R. A. Jones, E. J. Groen, H. K. Shorrock, F. M. Lane, Y. Zheng, D. L. Sherman, P. J. Brophy, T. H. Gillingwater, Restoration of SMN in Schwann cells reverses myelination defects and improves neuromuscular function in spinal muscular atrophy. *Hum. Mol. Genet.* **25**, 2853–2861 (2016).
39. G. V. Michailov, M. W. Sereda, B. G. Brinkmann, T. M. Fischer, B. Haug, C. Birchmeier, L. Role, C. Lai, M. H. Schwab, K. A. Nave, Axonal neuregulin-1 regulates myelin sheath thickness. *Science* **304**, 700–703 (2004).
40. C. Taveggia, G. Zanazzi, A. Petrylak, H. Yano, J. Rosenbluth, S. Einheber, X. Xu, R. M. Esper, J. A. Loeb, P. Shrager, M. V. Chao, D. L. Falls, L. Role, J. L. Salzer, Neuregulin-1 type III determines the ensheathment fate of axons. *Neuron* **47**, 681–694 (2005).
41. D. Riethmacher, E. Sonnenberg-Riethmacher, V. Brinkmann, T. Yamaai, G. R. Lewin, C. Birchmeier, Severe neuropathies in mice with targeted mutations in the ErbB3 receptor. *Nature* **389**, 725–730 (1997).
42. M. T. Woldeyesus, S. Britsch, D. Riethmacher, L. Xu, E. Sonnenberg-Riethmacher, F. Abou-Rebyeh, R. Harvey, P. Caroni, C. Birchmeier, Peripheral nervous system defects in erbB2 mutants following genetic rescue of heart development. *Genes Dev.* **13**, 2538–2548 (1999).
43. D. Wolpowitz, T. B. Mason, P. Dietrich, M. Mendelsohn, D. A. Talmage, L. W. Role, Cysteine-rich domain isoforms of the neuregulin-1 gene are required for maintenance of peripheral synapses. *Neuron* **25**, 79–91 (2000).
44. L. L. Crews, D. J. Wigston, The dependence of motoneurons on their target muscle during postnatal development of the mouse. *J. Neurosci.* **10**, 1643–1653 (1990).
45. A. R. Taylor, D. J. Gifondorwa, J. M. Newbern, M. B. Robinson, J. L. Strupe, D. Prevette, R. W. Oppenheim, C. E. Milligan, Astrocyte and muscle-derived secreted factors differentially regulate motoneuron survival. *J. Neurosci.* **27**, 634–644 (2007).
46. K. J. Swoboda, T. W. Prior, C. B. Scott, T. P. McNaught, M. C. Wride, S. P. Reyna, M. B. Bromberg, Natural history of denervation in SMA: Relation to age, SMN2 copy number, and function. *Ann. Neurol.* **57**, 704–712 (2005).
47. G. Sobue, Y. Matsuoka, E. Mukai, T. Takayanagi, I. Sobue, Pathology of myelinated fibers in cervical and lumbar ventral spinal roots in amyotrophic lateral sclerosis. *J. Neurol. Sci.* **50**, 413–421 (1981).
48. W. G. Bradley, P. Good, C. G. Rasool, L. S. Adelman, Morphometric and biochemical studies of peripheral nerves in amyotrophic lateral sclerosis. *Ann. Neurol.* **14**, 267–277 (1983).
49. B. T. Darras, T. O. Crawford, R. S. Finkel, E. Mercuri, D. C. De Vivo, M. Oskoui, E. F. Tizzano, M. M. Ryan, F. Muntoni, G. Zhao, J. Staropoli, A. McCampbell, M. Petrillo, C. Stebbins, S. Fradette, W. Farwell, C. J. Sumner, Neurofilament as a potential biomarker for spinal muscular atrophy. *Ann. Clin. Transl. Neurol.* **6**, 932–944 (2019).
50. Z. Xu, J. R. Marszalek, M. K. Lee, P. C. Wong, J. Folmer, T. O. Crawford, S. T. Hsieh, J. W. Griffin, D. W. Cleveland, Subunit composition of neurofilaments specifies axonal diameter. *J. Cell Biol.* **133**, 1061–1069 (1996).
51. A. Moosa, V. Dubowitz, Postnatal maturation of peripheral nerves in preterm and full-term infants. *J. Pediatr.* **79**, 915–922 (1971).
52. P. B. Kang, *The Clinical Neurophysiology Primer*, A. S. Blum, S. B. Rutkove, Eds. (Humana Press, 2007).
53. A. Moosa, V. Dubowitz, Motor nerve conduction velocity in spinal muscular atrophy of childhood. *Arch. Dis. Child.* **51**, 974–977 (1976).
54. T. Imai, R. Minami, M. Nagaoka, Y. Ishikawa, K. Kameda, M. Okabe, H. Matsumoto, Proximal and distal motor nerve conduction velocities in Werdnig-Hoffmann disease. *Pediatr. Neurol.* **6**, 82–86 (1990).
55. D. S. T. Kariyawasam, J. S. Russell, V. Wiley, I. E. Alexander, M. A. Farrar, The implementation of newborn screening for spinal muscular atrophy: The Australian experience. *Genet. Med.* **22**, 557–565 (2019).
56. K. Vill, H. Kolbel, O. Schwartz, A. Blaschek, B. Olgemoller, E. Harms, S. Burggraf, W. Roschinger, J. Durner, D. Glaser, U. Nennstiel, B. Wirth, U. Schara, B. Jensen, M. Becker, K. Hohenfellner, W. Muller-Felber, One year of newborn screening for SMA—Results of a German pilot project. *J. Neuromuscul. Dis.* **6**, 503–515 (2019).
57. A. Rashnonejad, G. Amini Chermahini, C. Gunduz, H. Onay, A. Aykut, B. Durmaz, M. Baka, Q. Su, G. Gao, F. Ozkinay, Fetal gene therapy using a single injection of recombinant AAV9 RESCUED SMA phenotype in mice. *Mol. Ther.* **27**, 2123–2133 (2019).
58. J. Gerdts, D. W. Summers, J. Milbrandt, A. DiAntonio, Axon self-destruction: New links among SARM1, MAPKs, and NAD+ metabolism. *Neuron* **89**, 449–460 (2016).
59. T. T. Le, L. T. Pham, M. E. Butchbach, H. L. Zhang, U. R. Monani, D. D. Coovert, T. O. Gavrilina, L. Xing, G. J. Bassell, A. H. Burghes, SMNΔ7, the major product of the centromeric survival motor neuron (SMN2) gene, extends survival in mice with spinal muscular atrophy and associates with full-length SMN. *Hum. Mol. Genet.* **14**, 845–857 (2005).
60. C. G. Carlson, J. Rutter, C. Bledsoe, R. Singh, H. Hoff, K. Bruemmer, J. Sesti, F. Gatti, J. Berge, L. McCarthy, A simple protocol for assessing inter-trial and inter-examiner reliability for two noninvasive measures of limb muscle strength. *J. Neurosci. Methods* **186**, 226–230 (2010).
61. C. M. Simon, M. Van Alstyne, F. Lotti, E. Bianchetti, S. Tisdale, D. M. Watterson, G. Z. Mentis, L. Pellizzoni, Stasimon contributes to the loss of sensory synapses and motor neuron death in a mouse model of spinal muscular atrophy. *Cell Rep.* **29**, 3885–3901.e5 (2019).
62. C. d'Ydewalle, D. M. Ramos, N. J. Pyles, S. Y. Ng, M. Gorz, C. M. Pilato, K. Ling, L. Kong, A. J. Ward, L. L. Rubin, F. Rigo, C. F. Bennett, C. J. Sumner, The antisense transcript SMN-AS1 regulates SMN expression and is a novel therapeutic target for spinal muscular atrophy. *Neuron* **93**, 66–79 (2017).
63. J. Vandesompele, K. De Preter, F. Pattyn, B. Poppe, N. Van Roy, A. De Paepe, F. Speleman, Accurate normalization of real-time quantitative RT-PCR data by geometric averaging of multiple internal control genes. *Genome Biol.* **3**, RESEARCH0034 (2002).

Acknowledgments: We would like to express our profound gratitude for the generosity and altruism of donors and their families, whose gifts of tissues serve an integral role in advancing medical research and education. We thank our colleagues who referred patients including J. Bradsema, G. Tennekoon, S. Al-Zaidy, R. Shell, N. Kuntz, and C. DiDonato, among others, and the numerous pathologists with whom we have worked, including J. Hooper, who leads the rapid autopsy program at Johns Hopkins Hospital. We thank A. Gupte for statistics analysis and K. Brown, C. Cooke, and M. Delannoy for EM technical support. We acknowledge the support of The Living Legacy Foundation of Maryland, an organization that works with donor families to honor their loved ones through the donation of organs and tissue for transplantation, education, and research. Some human tissues were received from the NIH NeuroBioBank at the University of Maryland (Baltimore, MD). We would also like to thank our colleagues L. Feltri, M. Farah, A. Hoke, M. Polley, and the late J. Griffin for their advice and expertise. **Funding:** This work was supported by funding from the SMA Foundation, The SMA Research Team, Cure SMA, and the NIH (R01 NS09677 and R01 NS062269) to C.J.S.; from NIH (R25 GM109441) to C.H.; from NIH (R01 NS078375 and R01 AA027079) to G.Z.M.; and from NICHD (R01-HD69045) to K.J.S. **Author contributions:** L.K., D.O.V., C.M.S., C.W.H., C.M.L., M.W., N.A.N., T.O.C., G.Z.M., and C.J.S. designed the research studies. L.K., D.O.V., C.M.S., C.W.H., N.D., J.H.P., C.M.P., X.X., Z.A.K., C.C.G., M.C., C.D., M.P., T.O.C., G.Z.M., and C.J.S. conducted experiments. L.K., D.O.V., C.M.S., C.W.H., N.D., J.H.P., C.M.P., X.X., Z.A.K., C.C.G., C.D., M.P., T.O.C., G.Z.M., and C.J.S. acquired data. L.K., D.V., C.M.S., D.M.R., M.P., M.W., G.Z.M., and C.J.S. analyzed data. C.D., C.M.L., K.J.S., M.W., X.Z., and N.A.N. provided reagents and samples for the study. L.K., C.M.S., D.M.R., T.O.C., G.Z.M., and C.J.S. wrote the manuscript. L.K., C.M.S., D.M.R., A.H.S., N.A.N., T.O.C., G.Z.M., and C.J.S. critically revised the manuscript. **Competing interests:** M.P. is an employee of Biogen. A.H.S. is an employee of F. Hoffmann-La Roche Ltd. X.Z., N.N., and M.W. are employees of PTC Therapeutics Inc., a biotechnology company. In connection with such employment, the authors receive salary, benefits, and stock-based compensation, including stock options, restricted stock,

other stock-related grants, and the right to purchase discounted stock through PTC's employee stock purchase plan. K.J.S. receives grant support from Biogen and Cure SMA. C.J.S. receives grant support from Roche Ltd. and has served as a paid advisor, consultant, and/or speaker to the SMA Foundation, Biogen, Ionis Pharmaceuticals, PTC Therapeutics, Roche/Genentech, and AveXis. This arrangement has been reviewed and approved by the Johns Hopkins University in accordance with its conflict of interest policies. All other authors declare that they have no competing interests. **Data and materials availability:** SMN-C8 was synthesized by H. Ratni, F. Hoffmann–La Roche Ltd., and shipped to JHU under a material transfer agreement. All the data are present in the main text or in the Supplementary Materials.

Submitted 13 March 2020
Accepted 18 September 2020
Published 27 January 2021
10.1126/scitranslmed.abb6871

Citation: L. Kong, D. O. Valdivia, C. M. Simon, C. W. Hassinan, N. Delestrée, D. M. Ramos, J. H. Park, C. M. Pilato, X. Xu, M. Crowder, C. C. Grzyb, Z. A. King, M. Petrillo, K. J. Swoboda, C. Davis, C. M. Lutz, A. H. Stephan, X. Zhao, M. Weetall, N. A. Naryshkin, T. O. Crawford, G. Z. Mentis, C. J. Sumner, Impaired prenatal motor axon development necessitates early therapeutic intervention in severe SMA. *Sci. Transl. Med.* **13**, eabb6871 (2021).

Science Translational Medicine

Impaired prenatal motor axon development necessitates early therapeutic intervention in severe SMA

Lingling Kong, David O. Valdivia, Christian M. Simon, Cera W. Hassinan, Nicolas Delestrée, Daniel M. Ramos, Jae Hong Park, Celeste M. Pilato, Xixi Xu, Melissa Crowder, Chloe C. Grzyb, Zachary A. King, Marco Petrillo, Kathryn J. Swoboda, Crystal Davis, Cathleen M. Lutz, Alexander H. Stephan, Xin Zhao, Marla Weetall, Nikolai A. Naryshkin, Thomas O. Crawford, George Z. Mentis and Charlotte J. Sumner

Sci Transl Med **13**, eabb6871.
DOI: 10.1126/scitranslmed.abb6871

The sooner, the better

Gene therapy approaches hold promise for the treatment of spinal muscular atrophy (SMA). However, these therapies showed that variable clinical response and earlier age of treatment initiation are associated with better outcome. Now, Kong *et al*. studied the pathophysiology of SMA to identify the best approach to maximize treatment efficiency. The authors used tissue from patients and a mouse model and identified developmental delay of motor neuron axons already in the fetus and subsequent early postnatal cell death. In utero therapeutic intervention prevented motor neuron degeneration and improved axonal function and motor behavior in mice. The results suggest that fetal treatment might increase the efficacy of current therapies for treating SMA.